Global Response of the Ionosphere to Atmospheric Tides Forced from Below: Recent Progress Based on Satellite Measurements

Global Tidal Response of the Ionosphere

Dora Pancheva · Plamen Mukhtarov

Abstract This paper provides an overview on the recent progress in studying the ionospheric response to atmospheric tides forced from below. The global spatial structure and temporal variability of the atmospheric temperature tides and their ionospheric responses are considered on the basis of modern satellite-board data (COSMIC and TIMED). The tidal waves from the two data sets have been extracted by one and the same data analysis method. The similarity between the lower thermospheric temperature tides and their ionospheric responses provides evidence for confirming the new paradigm of atmosphere-ionosphere coupling. This paper provides also new experimental results which give an explanation why the WN4 and partly WN3 longitude structures are so prominent pattern in the ionosphere. These results present evidence indicating that the WN4 (WN3) structure is not generated only by the DE3 (DE2) tide as it has been often assumed. The DE3 (DE2) tide remains the leading contributor, but the SPW4 and SE2 (SPW3, DW4 and SE1) waves have their effects as well in a way that the ionospheric response becomes almost double (1.5 time stronger). The paper presents also the global distribution and temporal variability of the sun-synchronous 24-h (DW1), 12-h (SW2) and 8-h (TW3) electron density oscillations. It has been shown that while the latitude and altitude structure of the ionospheric SW2 response is predominantly shaped by the migrating SW2 tide forced from below the DW1 response is mainly due to daily variability of the photo-ionization. The peculiar vertical structure of the ionospheric TW3 response, that shows downward/upward phase progression, calls for further study of the physical processes shaping this ionospheric response.

Keywords Nonmigrating tides · Ionospheric response · Modulated vertical plasma drift · "Fountain effect"

1 Introduction

The conventional sources of ionospheric structure and variability are related to changes in solar radiative output and geomagnetic activity, together with the subsequent response of

D. Pancheva (✉) · P. Mukhtarov
Geophysical Institute, Bulg. Acad. Sciences, Sofia, Bulgaria
e-mail: dpancheva@geophys.bas.bg

the thermosphere and ionosphere system and interaction between the components. The high sensitivity of the ionosphere to the external forcing causes its significant variability on time scales ranging from minutes to a solar cycle. To understand and forecast such variability is one of the main tasks of space weather research. Often, and especially recently when the level of solar activity is very low, quite large day-to-day changes of the ionosphere have been observed. With the recent accumulation of satellite measurements, attention is now being directed towards investigating the impact of the processes from below and particularly the wave forcing from the lower atmosphere.

The low-latitude ionospheric morphology is greatly affected by the electric fields and neutral winds which define its dependence on latitude, longitude and local time. The neutral wind and electric field effects on the ionosphere are variable with geomagnetic field configuration (magnetic field strength, magnetic declination, and displacement of the geomagnetic equator from the geographic equator) and this is the reason for many years the ionospheric longitudinal variations to be understood mainly in the context of geomagnetic field configuration (West and Heelis 1996; Thuillier et al. 2002; Kil et al. 2006). Recently, however, various ionospheric observations have shown the development of longitudinal wave-like patterns (as wave number three (WN3), or wave number four (WN4) structures) that cannot be explained by the geomagnetic field configuration. The wave-like longitudinal plasma density pattern was first reported by topside soundings from the Russian satellite Intercosmos-19 (Kochenova 1987, 1988; Karpachev 1988). Intercosmos-19 observed the formation of four peaks in plasma density (WN4 structure at a fixed local time frame) over the magnetic equator (Benkova et al. 1990), but the focus of this study was on the displacement of the geomagnetic equator from the geographic equator and the hemispheric asymmetry induced by neutral winds.

It has been mentioned above that the Earth's ionosphere is closely connected to atmospheric waves propagating from below. Among them are solar thermal tides which are global-scale atmospheric oscillations in all atmospheric fields, including wind, temperature, density and pressure, with periods that are subharmonics of a solar day. These waves profoundly affect the large-scale dynamics of the mesosphere and lower thermosphere (MLT) where they attain large amplitudes and dominate the large-scale atmospheric fields. Like other waves the tidal components grow in amplitude with increasing altitude since atmospheric density decreases and energy must be conserved. Generally, the tidal amplitudes are the largest of all the atmospheric oscillations in the MLT region, including also gravity and planetary waves. The major source of forcing at tidal periods in the lower and middle atmosphere is atmospheric heating due to absorption of solar radiation by zonally symmetric atmospheric components as stratospheric ozone and tropospheric water vapor. The resulting atmospheric variations are reflected in migrating tides which propagate with the apparent motion of the Sun to a ground-based observer, i.e. they are a function of local time alone (Chapman and Lindzen 1970). Other sources may contribute to tidal variations that depend explicitly on longitude and in this way resulting in nonmigrating tides (all tides propagating eastward, zonally symmetric tides and those propagating westward but with a different phase speed from that of the apparent motion of the Sun). It is now generally accepted that nonmigrating tides arise from at least two mechanisms: zonally asymmetric thermal forcing (surface topography, geographically varying heat sources, variation of solar heating with longitude) and nonlinear interactions between migrating tides and stationary planetary waves (SPWs) (Angelats i Coll and Forbes 2002; Pancheva et al. 2009a). For instance, the release of latent heat by deep convective clouds is dependent on universal time (UT), longitude, latitude and season hence it is a possible source that could generate a nonnegligible tidal migrating and nonmigrating response in the MLT (Hamilton 1981; Williams and Avery 1996;

Hagan 1996; Hagan and Forbes 2002, 2003; Oberheide et al. 2002). McLandress and Ward (1994) suggested that the interaction of a zonally asymmetric distribution of the gravity waves interacting with migrating tides could also generate nonmigrating tides.

Due to increasing eddy and molecular dissipation the lower thermosphere is a region where the atmospheric tides propagating from below usually damp. Dissipating tides deposit net momentum and energy into the mean flow and thus modify the mean circulation at these altitudes. They can also mix the atmospheric species there or nonlinearly interact with other waves generating additional wave activity (Forbes et al. 1993). Through impacting the wind fields and mixing, the tides can affect the density of different neutral species like NO, O, CO_2 and O_3 and in this way affect the energy budget either by radiating, or by absorbing solar radiation. The tides penetrating in the ionospheric E-region ($\sim$100–170 km) can also affect the overlying ionosphere F-region by the so called "E-region wind dynamo". In this way the neutral dynamics renders the lower thermosphere the strongest driver from below of the ionosphere F-region. The "E-region wind dynamo" is composed by the following sequence of processes (Richmond 1995; Heelis 2004; Forbes et al. 2008): (i) the tidal winds move positive ions through collisions while electrons remain fixed to magnetic field lines due to their high gyrofrequency/collision frequency ratio; (ii) an electric current is thus induced; (iii) in order to maintain nondivergent flow of total electric current in accord with Maxwell's steady-state equations, polarization electric fields are set up almost instantaneously; (iv) these polarization electric fields are transmitted from the low- and middle-latitude E-region to the equatorial F-region along equipotential magnetic field lines and (v) there, they modulate the background zonal electric field and the accompanying $E \times B$ vertical drift that redistributes plasma upward and poleward to produce the equatorial ionization anomaly (EIA) near $\pm$15–20° dip latitude. Additionally, recent investigations showed that the atmospheric tides can propagate also directly up to thermospheric heights (Oberheide et al. 2009). Therefore, either through complex coupling mechanisms or through direct propagation, the MLT tides can affect the whole ionosphere-thermosphere system.

Recent studies based on the observations made by the Sounding of the Atmosphere using Broadband Emission Radiometry (SABER) and the TIMED Doppler Interferometer (TIDI) instruments on the Thermosphere-Ionosphere-Mesosphere-Energetics and Dynamics (TIMED) satellite have provided new insight into tidal fields and revealed the global distribution and climatology of the most important tidal components in temperature and neutral winds respectively (e.g., Zhang et al. 2006; Huang et al. 2006a, 2006b; Forbes et al. 2006, 2008; Oberheide et al. 2007; Oberheide and Forbes 2008; Mukhtarov et al. 2009; Xu et al. 2009; Pancheva et al. 2009b, 2010a; Pancheva and Mukhtarov 2011). Some of the above mentioned studies clearly suggested that the nonmigrating tides are much larger than previous anticipated and often exceed the migrating tide counterparts in the lower thermosphere (e.g., Zhang et al. 2006; Forbes et al. 2006, 2008; Oberheide et al. 2006, 2007; Pancheva et al. 2010b). The nonmigrating tides give rise to longitudinal variations in local time structures of neutral winds and temperatures in the MLT region. Through coupling mechanisms (such as the wind dynamo), the nonmigrating tides can play an important role in generating the longitudinal variability in the ionosphere. In this way, a special attention has been paid recently on the nonmigrating tides as a possible link between the troposphere and ionosphere.

The last several years have seen an abundance of new observational evidence illustrating terrestrial weather impacts on the ionosphere. The evidence has emerged from different measurements and all of them unambiguously display manifestations of lower atmospheric dynamics on the upper atmosphere and ionosphere. Such illustrations are various ionospheric

observations which show the development of longitudinal WN3 or WN4 structures which are suggested to be caused by different atmospheric tides. Sagawa et al. (2005) observed four enhanced longitude regions of the nighttime airglow intensity in the EIA and pointed out that the WN4 longitudinal structure of the plasma density is most probably forced by the atmospheric tides. The authors suggested that non-migrating tides that propagate from lower altitudes to the E region can modulate the E-region dynamo electric field and produce the observed WN4 density pattern in the F region. Later Immel et al. (2006) and England et al. (2006a) specified that the diurnal eastward propagating zonal wave number 3 (DE3, D corresponds to diurnal tide and E to eastward propagation) tide is responsible for the generation of the ionospheric WN4 density structure. We note that when viewed at a fixed local time the DE3 wave is seen as four maxima on longitude in all tidal fields. As evidence of modulation in the dynamo, a WN4 structure has been observed in $E \times B$ plasma drift (Hartman and Heelis 2007; Kil et al. 2007, 2008; Ren et al. 2008, 2009) and in the equatorial electrojet (EEJ) (England et al. 2006b; Lühr et al. 2008). The satellite observations of different ionospheric and thermospheric parameters, such as: total electron content (TEC), the electron temperature, F-region zonal neutral wind and neutral mass density, the ionospheric F2 layer height (h_mF2), also have shown WN4 longitude structures (e.g., Lin et al. 2007a, 2007b; Lühr et al. 2007; Häusler and Lühr 2009; Wan et al. 2008; Fejer et al. 2008; Bankov et al. 2009; Liu et al. 2009; Pancheva and Mukhtarov 2010).

Model simulations support the causal link between DE3 tide and WN4 ionospheric longitude structure. Hagan et al. (2007) used the GSWM tidal winds as input to the Thermosphere-Ionosphere-Mesosphere-Electrodynamics General Circulation Model (TIME-GCM) and identified the DE3 zonal wind as the cause of the formation of WN4 structure. Jin et al. (2008) and Ren et al. (2010) on the basis of electrodynamic simulations pointed out also that the charge separation induced by the Hall current driven by DE3 tide winds causes the WN4 structure in the E-region zonal electric field. With the influence of the coupling of ionospheric electric fields along the highly conducting magnetic field lines Ren et al. (2010) found that the symmetric wind component of DE3 tide plays a more important role in the WN4 structure in the vertical $E \times B$ plasma drift than does the antisymmetric component. For understanding the atmospheric vertical coupling, global first-principal models treating both atmospheric and ionospheric regions, like the above mentioned TIME-GCM (Roble 1996) are quite useful. Such models are: the TIME-GCM/CCM3, which couples TIME-GCM and a lower atmospheric model of the Climate Community Model version 3 (CCM3) (Roble 2000), the Whole Atmosphere Model and a Global Ionosphere Plasmosphere Model (Fuller-Rowell et al. 2008), and the model called GAIA which combines three models, that is, a whole atmospheric GCM, an ionospheric model and an electrodynamics model (Jin et al. 2011).

All the above mentioned studies clearly indicated that the WN4 longitude structure is a very prominent feature of the low-latitude ionosphere-thermosphere system that in general can be reproduced by the models. So far however, the ionospheric wave-like longitude structures have been investigated only at fixed local times (LT) most probably because they were observed by quasi-sun-synchronous satellites. In this case however the observed structure cannot be directly related to a certain tidal component. For example, if we consider only diurnal and semidiurnal tides, the WN4 structure can be forced by: DE3, DW5, SW6, SE2 and SPW4 (according to the standard nomenclature S corresponds to semidiurnal tide, while W to westward propagation; SPW means the stationary planetary wave) and the WN3 structure by: DW4, DE2, SW5, SE1 and SPW3 (Häusler and Lühr 2009) and any of these waves could in principal contribute to the ionosphere WN4/WN3 variability. Its relative importance, of course, depends on its magnitude in

the E-region and characteristics such as latitudinal shape and vertical wavelength (Ober-heide et al. 2011). Usually the annual and LT variations of the WN4 structure indicate the prevailing effect of the DE3 tide, but the contribution of the other aforementioned tides and SPW4 cannot be excluded. The formation mechanism of the WN3 structure, that is observed mainly during the Northern hemisphere (NH) winter (England et al. 2009; Pancheva and Mukhtarov 2010), has not yet been clarified. However Pedatella et al. (2008) have already made the point that the WN3 is mainly due to the DE2 by comparing the CHAMP CTR data to the TIDI neutral wind tides in the E-region. Similar to the WN4 struc-ture, in this case also we cannot exclude the contribution of the other above mentioned tides and SPW3.

The basic aim of the present paper is to study the global distribution and temporal vari-ability of the ionospheric response to atmospheric tides forced from below. Only when the ionospheric response to each wave forced from below is known then the relative contribution and importance of the above mentioned waves in generating the ionospheric longitudinal WN4 or WN3 structures can be studied. For this purpose the Constellation Observing Sys-tem for Meteorology, Ionosphere, and Climate (COSMIC) electron densities at given heights are utilized in order to define the ionospheric wave response. The wave forcing from below, e.g. the lower thermospheric waves are defined by using the SABER/TIMED temperatures. The period of time 1 October 2007–31 March 2009 is considered in the present study; it covers solar minimum conditions when the tidal damping in the lower thermosphere should be weaker because of the reduced tidal dissipation.

2 Observations and Method for Data Analysis

2.1 COSMIC Electron Density Profiles Data

The electron density profiles employed in this study were retrieved by the advanced GPS receivers on board of COSMIC satellites using a radio occultation (RO) inversion technique (Cheng et al. 2006). Six identical microsatellites constitute the COSMIC constellation sys-tem. They were initially launched (on April 2006) into the same orbit, and then during the following 13 months, they were gradually spread to individual orbits at a higher altitude of about 800 km. Since late 2007, the satellites have operated on their final orbits with the inclination of 72° and 30° separation in longitude. Each COSMIC satellite has a GPS occul-tation experiment payload, performing the radio occultation observations in the ionosphere. The details of the inversion technique applied to invert the COSMIC occultation soundings to ionospheric electron density profiles are given by Schreiner et al. (1999) and Lei et al. (2007). The COSMIC satellites now provide approximately 24 h of LT coverage globally and about 2200 vertical electron density profiles per day. The ionospheric measurements of COSMIC have been assessed by comparing with ground-based measurements and model prediction (Lei et al. 2007). The advantages of making use of the COSMIC-measured data to study the F-region electron density variability are nearly uniformly global distribution of the electron density profiles with sufficiently fine height and horizontal resolutions, which cannot be achieved for the data taken from the conventional ground-based ionosonde net-works. In this way the COSMIC GPS occultation experiment has proven to be a powerful tool in probing vertical profiles of the ionospheric electron density by its global-coverage observations.

The electron density data downloaded from the web site http://cosmic-io.cosmic.ucar.edu/cdaac/ had to be preprocessed before using them for the wave analysis. The prepro-cessing steps included removing: (i) negative values of the electron densities; (ii) electron

densities corresponding to plasma frequencies larger than 20 MHz (in this study the electron density is measured by its plasma frequency in MHz); and (iii) spurious spikes. The electron density data from September 2007 to April 2009 are used in this study. The data were sorted out according to: (i) latitude, at each 10° between 80°S and 80°N; (ii) longitude, at each 15°; (iii) altitude, at each 25 km between 100 and 800 km; and (iv) time, for each UT hour. Finally, for each latitude and height the electron density data were arranged into a matrix with 24 columns (this is the longitude with a step of 15°) and a number of rows equal to the length of the considered period of time in hours. It has been mentioned that the ionospheric tidal response will be studied by considering the electron densities at fixed altitudes between 100 and 800 km. Besides them the F-region is characterized also by its maximum electron density (f_oF2), the h_mF2 and the bottom and top coefficients describing the respective vertical gradients of the electron density, called slope coefficients. The parameters f_oF2 and h_mF2 are defined by their real values from the profile, however to avoid the influence of the sporadic E_s layers they are found for altitudes higher than 175 km. The bottom and top slope coefficients are defined as scale heights B calculated for 50 km below and 100 km above the h_mF2 as the electron density profile is approximated by:

$$N(h) = N_m \sec h^2\left(\frac{h - h_m}{2B}\right) = \frac{4N_m}{(1 + \exp(\frac{h-h_m}{B}))^2} \exp\left(\frac{h - h_m}{B}\right) \tag{1}$$

where B is a scale height and N and N_m are electron density at a given height h and at electron density peak height h_m respectively. The above approximation is used in modeling electron density profiles (Radicella and Leitinger 2001) or in the reconstruction of the electron density profiles in the topside ionosphere and plasmosphere (Stankov et al. 2003).

2.2 SABER Temperature Data

The TIMED satellite was launched on 7 December 2001 and the SABER instrument began making observations in January 2002. It measures CO_2 infrared limb radiance from approximately 20 km to 120 km altitude and kinetic temperature profiles are retrieved over these heights using LTE radiative transfer in the stratosphere and lowest part of the mesosphere (up to ∼60 km), and a full non-LTE inversion in the MLT (Mertens et al. 2001, 2004). SABER views the atmosphere at an angle of 90° with respect to the satellite velocity vector in a 625 km height and 74° inclination orbit so that the latitude coverage on a given day extends from about 53° in one hemisphere to 83° in the other. About every 60 days, the latitude ranges flip as the spacecraft yaws to keep the instrument on the anti-sunward side of the spacecraft. In this way high latitude data are available only in 60-day segments, with no information for the 60 days preceding or following. This is the reason not to generate results poleward of 50°. The TIMED orbit precesses and covers 12 hours of LT in each 60-day yaw period, so that ascending and descending data together give almost 24 hours of LT sampling.

Our results are derived from the latest Version 1.07 of the SABER data, which were downloaded from the web site: http://saber.gats-inc.com. The details about the assessment of the SABER temperatures can be found in Remsberg et al. (2008). We use temperature data from September 2007 to April 2009 in order to study the temporal variability and global spatial structure of the atmospheric tides forced from below. The data were averaged into 5 km altitude and 10° latitude bins and each bin was independently fit. We work in UT and for each altitude (from 20 to 120 km in 5 km steps) and latitude (from 50°S to 50°N in 10° steps) the data were arranged into a matrix with 24 columns (this is the longitude with a step of 15°) and the number of rows is equal to the length of the considered period of time in hours.

2.3 Method for Extracting Waves from COSMIC Electron Density

The basic aim of this study is to obtain the global spatial structure and temporal variability of the ionospheric response to the known waves (defined by SABER temperature measurements) which propagate from the troposphere and reach the lower thermosphere. This means that we have to separate from the COSMIC electron density data the ionospheric oscillations with known periods and zonal structures. The known waves are solar tides with periods of 24, 12 and 8 hours and with zonal wavenumbers up to 4, as well as planetary waves (stationary and propagating) with zonal wavenumbers up to 4. The preliminary 2D spectral analysis of the COSMIC and SABER data revealed relatively weak zonally travelling planetary waves during the considered period of time. Only the zonally symmetric waves (zonal wavenumber zero) possessed large amplitudes, but it was found that they are due to external forcing (Lei et al. 2008). Therefore, the wanted tidal and planetary wave ionospheric responses are obtained by using the same method as that used for deriving the atmospheric waves from the SABER temperatures. This data analysis method is described in detail by Pancheva et al. (2009c). The advantages of this method are as follows: (i) to avoid the constraint of sampling uniformity, instead of a Fourier transform a linear two-dimensional (time-longitude) least squares fitting technique is used to extract the waves, (ii) to avoid a possible distortion of the weaker planetary waves by the stronger ones, all significant planetary waves are extracted simultaneously from the data, and (iii) to avoid the aliasing between the nonmigrating tides and the SPWs or between the migrating tides and the zonal mean, the tides (migrating and nonmigrating) are extracted simultaneously with the planetary waves.

Because the same method is used for the COSMIC and SABER data, and because it takes SABER 60 days to sample 24 hours in LT by combining ascending and descending data together, the length of the sliding window used for performing the 2D least-squares fitting procedure is 60 days. The 60-day window is then moved through the time series with steps of 24 hours in order to obtain the daily values of the wave characteristics for period of time October 2007–March 2009. Only continuous latitudinal results are considered in this study; for COSMIC electron density data, they are between 70°S and 70°N while for SABER temperature data, they are between 50°S and 50°N. It is worth noting that the use of a 60-day segment gives too smoothed ionospheric tidal response. However, because the emphasis is on the ionospheric response at low and middle latitudes, this helps to obtain reliable results as the number of the COSMIC measurements at low latitudes is smaller than that at high latitudes. The waves at given latitude and height are extracted by using the following expression:

$$\Theta(t,l) = \Theta_0 + \Theta_r t + \sum_{s=1}^{4} B_s \cos\left[\frac{2\pi}{360}sl - \frac{2\pi}{360}\psi_s\right]$$

$$+ \sum_{k=1}^{3}\sum_{s=-4}^{4} C_{ks} \cos\left[k\frac{2\pi}{24}t - \frac{2\pi}{360}sl - \frac{2\pi}{360}\gamma_{ks}\right] \tag{2}$$

where t is time in hours counted from 0 UT on 1 October, l—longitude in degrees, s—wavenumber, k—number of the diurnal harmonic. The eastward (westward) propagation corresponds to $s > 0$ ($s < 0$). The four terms on the right hand side of the above expression are as follows: (i) the mean ionospheric parameter Θ_0 (zonal and time mean), (ii) a linear term with coefficient Θ_r responsible for zonally symmetric variations with period longer than 60 days; this term includes a possible effect of the ionospheric semiannual variability,

(iii) stationary waves with amplitudes B_s and phases ψ_s, and (iv) 24-h, 12-h and 8-h tides with amplitudes C_{ks} and phases γ_{ks}. In the above expression the phases of the tides are defined as the time of the wave maxima at zero longitude and are presented in degrees, while the phase of the stationary wave—as the longitude of the wave maximum.

It is important to note that the results for the COSMIC electron density and SABER temperature sun-synchronous 24-h (DW1), 12-h (SW2) and 8-h (TW3, T corresponds to terdiurnal tide) tides have different nature. While in the SABER temperatures they are the migrating tides, those in the COSMIC electron density are produced by a combination of the diurnal variability of the photo ionization, which depends on the solar zenith angle, and the effect of the migrating tides forced from below. Therefore, by using the above mentioned data analysis method, the effect of the daily variability of the ionization cannot be separated from the effect of the migrating tides. In this study we will make an attempt to estimate which of the two effects is prevailing in the observed ionospheric DW1, SW2 and TW3 responses. The nonmigrating tidal effects in the COSMIC electron densities however, can be fully separated.

Because of the satellite data sampling pattern and the variability of the ionosphere particularly near the F-region maximum at low latitudes a very important problem in the ionospheric tidal response assessment is how to determine the reference noise level. For this purpose we use the same approach as that applied for the SABER satellite data and described in detail by Pancheva et al. (2009a). It is based on a method for generating of time series with a normal distribution by using of random number generator with an uniform probability distribution (Jeruchim et al. 2000). The generated in this way time series of random numbers will have a mean approaching zero and a standard deviation close to 1, i.e. white noise. This unit normal random time series can be further modified to have a particular mean and variance by multiplying with the given standard deviation and adding the mean.

As the WN4 ionospheric longitude structure related mainly to DE3 tide is particularly strong in August-September the results of the reference noise level analysis will be shown for this period of time. For each altitude and modified dip latitude (the clarification of the modified dip, or modip, latitude is given in the next section) 200 Gaussian hourly noise datasets with length of 61 days and with data sampling pattern, variance and mean as those of the true COSMIC electron density measurements were generated (Kong et al. 1998). Then the $2D$ spectral analysis in the periodic range of 3–30 hours was performed on the resulting noise datasets. The reference noise spectrum for each zonal wavenumber was calculated as an average spectrum. As an example for the reference noise spectra the result for the ionospheric parameter f_oF2 is shown in Fig. 1a, where the latitude structure of the noise spectrum for westward propagating waves with zonal wavenumber 2 (W2) is presented in the left plot while for eastward propagating waves with zonal wavenumber 2 (E2) is seen in the right plot. Both noise spectra do not reveal some particular peaks because of data sampling pattern and the ionospheric variability. An enhancement of the spectral power at modip latitude range of $\pm 30°$ is seen but the amplitudes of the randomly distributed peaks do not exceed 0.016 MHz for W2 and 0.018 MHz for E2. Similar results are obtained for the other zonal wavenumber f_oF2 noise spectra. Figure 1b shows the altitude structure of the electron density noise spectra over the equator; the left plot presents the noise spectrum for eastward propagating waves with zonal wavenumber 3 (E3) while the right plot presents that for westward propagating waves with zonal wavenumber 1 (W1). Again both noise spectra do not reveal some particular peaks; only an enhancement of the spectral power is seen between altitudes of ∼250–350 km with peaks which do not exceed 0.017 MHz for E3 and 0.018 MHz for W1. The results of this reference noise spectral analysis clearly indicated that because of the COSMIC data sampling pattern and the ionospheric variability there aren't
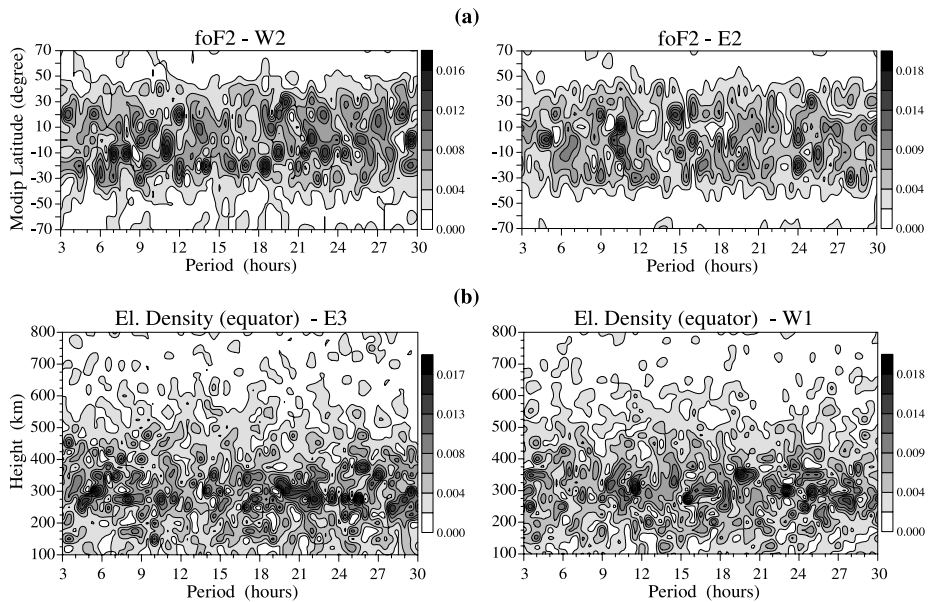
Fig. 1 (**a**) Latitude structure of the f_oF2 noise spectra in the periodic range of 3–30 hours for westward propagating waves with zonal wavenumber 2 (W2) (*left plot*) and for eastward propagating waves with zonal wavenumber 2 (E2) (*right plot*); (**b**) Altitude structure of the electron density noise spectra in the periodic range of 3–30 hours over the equator for eastward propagating waves with zonal wavenumber 3 (E3) (*left plot*) and for westward propagating waves with zonal wavenumber 1 (W1) (*right plot*)

revealed particular spectral peaks. The found low latitude amplification of the spectral f_oF2 noise power is related to the variability of the F-region maximum in the densest part of the ionosphere while the enhancement of the electron density noise spectral power between altitudes of ∼250–350 km reflects the diurnal variability of the F-region over the equator.

Similar analysis of that shown in Fig. 1 was done on each 60-day window (because a 60-day window is used for extracting the waves) for the considered altitudes and latitudes. On the average the obtained noise amplitudes did not exceed 0.018 MHz. Therefore, all COSMIC tidal waves extracted from a given 60-day window with amplitudes larger than 0.02 MHz are accepted as statistically significant.

3 COSMIC Response to Nonmigrating Tides

As it was mentioned, the ionospheric WN4 longitudinal structures are thought to reflect the effect of the tropospheric weather on the ionosphere because of the nonmigrating DE3 tide which is mainly forced by deep tropical convection (Hagan and Forbes 2002). Similarly, the ionospheric WN3 structure, which is pronounced usually in winter, has been associated with DE2 tide. In view of this our analysis will start with the ionospheric response to the above mentioned nonmigrating tides seen in the ionospheric parameter h_mF2, which is closely related to the vertical plasma drift and in this way is more sensitive to dynamics.
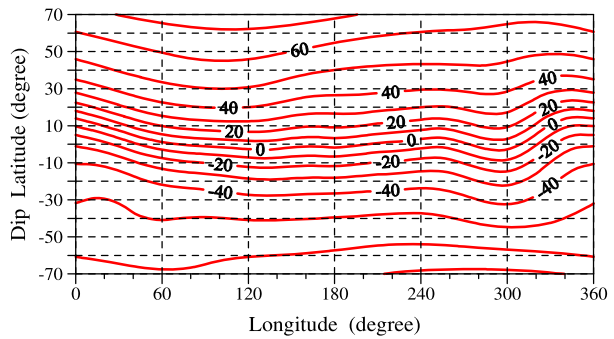
If the ionospheric WN4 and WN3 structures are driven by tides, coming from below, then similar pictures have to be observed between the SABER lower thermospheric DE3 and DE2 tides and their ionospheric counterparts. The upper row of plots in Fig. 2a shows
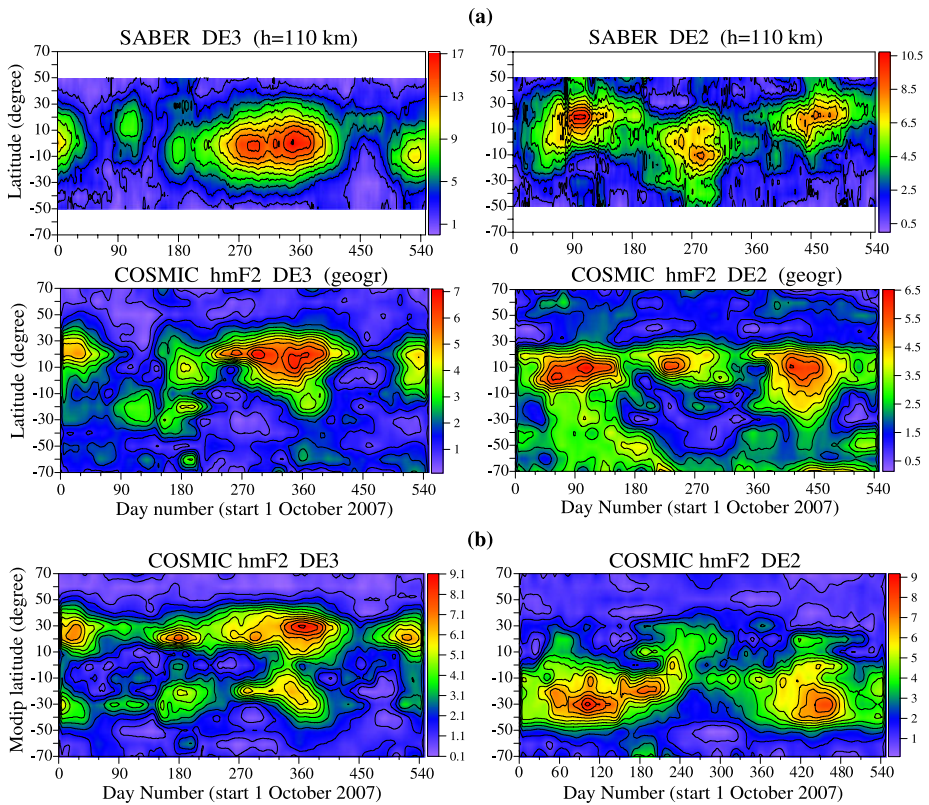
Fig. 2 (**a**) Latitude-time cross sections of the DE3 (*left column* of plots) and DE2 (*right column* of plots) tidal amplitudes seen in the SABER temperatures (*upper row* of plots, in Kelvin) and in the ionospheric h_mF2 (*bottom row* of plots, in km) for the period of time October 2007–March 2009; (**b**) The same as (**a**) but instead of geographic a modip latitude is used

the latitude ($\pm 50°$) structures of the SABER temperature DE3 (left plot) and DE2 (right plot) tides at 110 km altitude, while the bottom row of plots shows the latitude ($\pm 70°$) structures of their ionospheric responses seen in h_mF2. We note that both SABER and COSMIC results are in geographic latitudes. The similarity between the forcing from below (SABER tides, upper row of plots) and its ionospheric response (bottom row of plots) is remarkable. This strongly supports the causal link between the two phenomena. While the h_mF2 DE3 response prevails between June and October with maximum amplitude of ∼7 km that of DE2 response is pronounced mainly in winter (a secondary summer amplification as well) with amplitude of ∼6.5 km. The climatology of the SABER DE3 and DE2 tides (Pancheva et al. 2010b) indicated that while the DE3 is the predominant diurnal tide in the summer E-region (∼115 km height), the DE2 tide prevails during the winter. This defines their significant modulating effect on the vertical plasma drift/h_mF2 variability. The above result, reported by Pancheva and Mukhtarov (2010), is the first experimental evidence of the tidal coupling between lower atmosphere and ionosphere. It was possible because of using modern satellite-born (SABER and COSMIC) data effectively analyzed by one and the same method.

It has already been mentioned that the neutral wind and electric field effects on the ionosphere are at variance with the geomagnetic field configuration. That is why the distribution of the ionospheric parameters is usually presented in geomagnetic latitude instead of geographic one. Early investigations (reported, e.g., in Rawer 1984) demonstrated the benefit of using the modified dip latitude (modip), introduced by Rawer (1963), to describe the variability of the densest part of the ionosphere, particularly at mid and low latitudes. The modified dip (modip) latitude which is adapted to the real magnetic field, e.g., to the magnetic inclination (dip), is defined by: $\tan\mu = I/\sqrt{\cos\Phi}$, where μ is the modip latitude, I is the true magnetic dip (usually at a height of 350 km), and Φ is the geographic latitude. Modip equator is the locus of points where the magnetic dip (or inclination) is 0. In the equatorial zone, the lines of constant modip are practically identical to those of the magnetic inclination but as latitude increases they deviate and come nearer to those of constant geographical latitude. The poles are identical to the geographic ones (Azpilicueta et al. 2006). Figure 3 shows the relationship between the frequently used dip (black dash lines) and modip (thick red lines) latitudes. The modip isolines are denser in the low latitudes; this allows a more detailed representation of the ionospheric tidal responses at low and middle latitudes.

Figure 2b displays the h_mF2 DE3 (left plot) and DE2 (right plot) responses in modip latitude frame. In general, the main features of the DE3 and DE2 responses from Fig. 1a remain, however the amplitudes are larger in modip frame; in this case they reach ∼9 km. An important difference is seen however in modip frame; there is a splitting of the response at both sides of the dip equator particularly well evident for the DE3 response. The response is located near ±30° modip latitude, which is near ±10–20° dip latitude (see Fig. 3).

In order to study the spatial structure and particularly the vertical structure of the ionospheric DE3 and DE2 responses Mukhtarov and Pancheva (2011) utilized the COSMIC electron densities at given heights. Figure 4 shows the latitude (±70°) structure of the COSMIC DE3 (left column of plots) and DE2 (right column of plots) electron density responses at heights: 600 km (upper row of plots)), 400 km (middle row of plots) and 200 km (bottom row of plots). The latitude structure of the electron density responses show a splitting around a dip equator at 200 and 400 km heights, while at upper levels the splitting gradually disappears and the response moves toward the equator. This latitudinal structure indicates the role of the plasma drift in shaping the response: at 200 km and especially at 400 km the response is part of the "fountain effect" while at the upper levels, e.g. in the topside ionosphere, it is approximately confined over the dip equator. The latter feature is particularly well evident for the DE3 response. Figure 4 shows also that the strongest response for both tides produced by the "fountain effect" is observed near ±30° modip latitude. The response
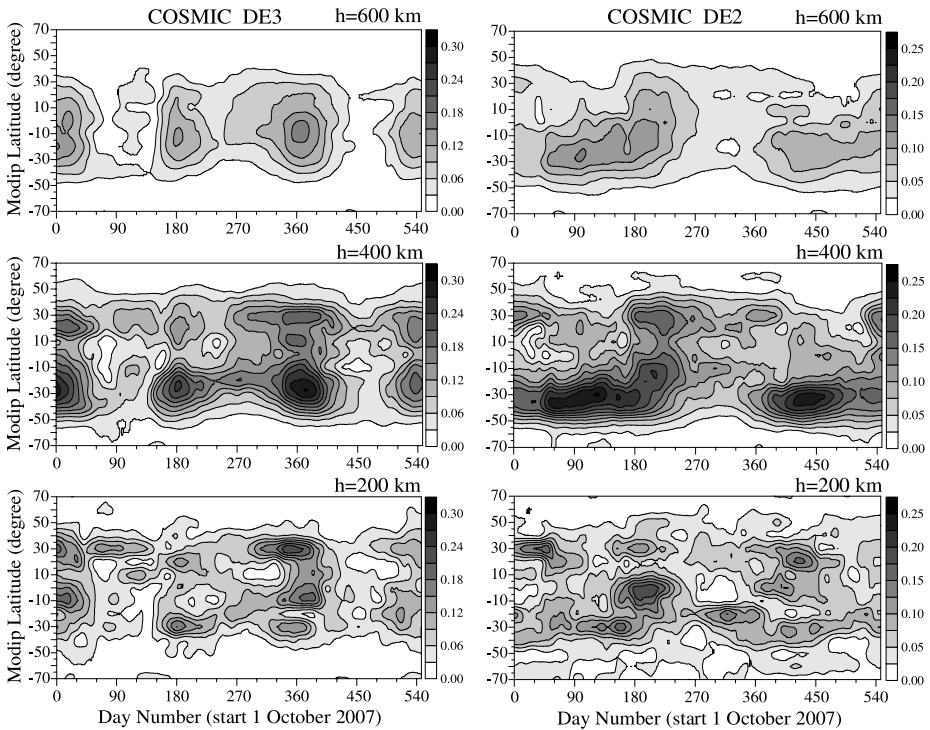
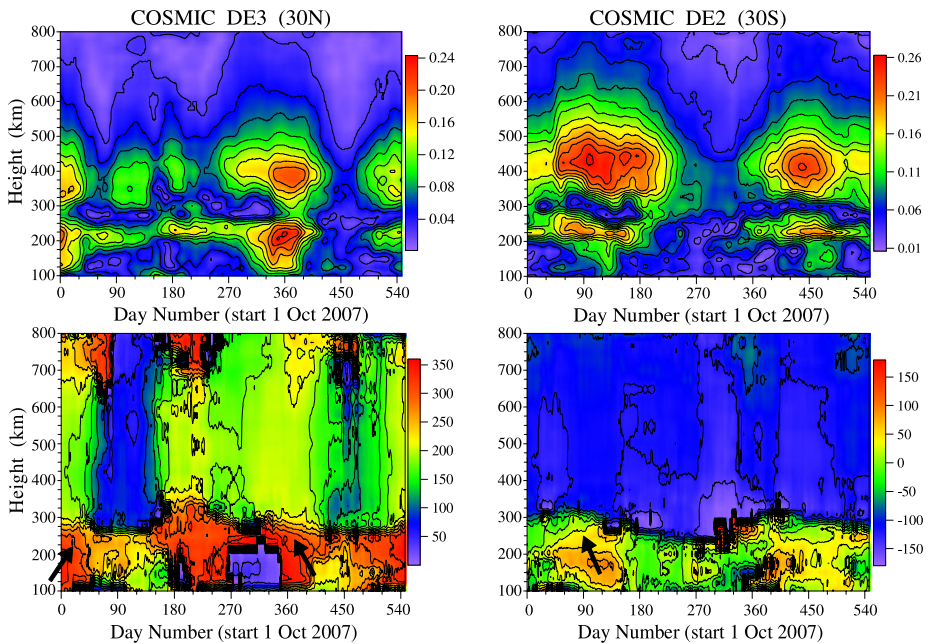**Fig. 4** Latitude structure (±70°) of the amplitudes in MHz of the electron density DE3 (*left column* of plots) and DE2 (*right column* of plots) responses at heights: 600 km (*upper row* of plots), 600 km (*middle row* of plots) and 200 km (*bottom row* of plots); all scales for DE3 and for DE2 are the same

at 200 km height is more complex; besides amplification near ±30° modip latitude it shows a response also close to the dip equator.

Figure 4 displays some difference between the COSMIC h_mF2 (Fig. 2a) and electron density DE3 responses: the electron density response in March, particularly up to 400 km height, is much stronger than that of the h_mF2 response. The reason is that while the h_mF2 response is mainly dependent on the dynamics of the thermosphere, the tidal response of the electron density depends on other factors as well. It is worth noting that, for example, the ratio of [O] and [N_2] that is controlled by the thermospheric circulation is the key parameter dominating the semiannual variation of the F-region anomaly at low latitudes with the greatest f_oF2 at equinox (Rishbeth et al. 2000). When the background electron density is higher then the DE3 electron density response also will be stronger.

Figure 5 shows the altitude structure of the amplitudes in MHz (upper row of plots) and phases in degrees (bottom row of plots) of the electron density DE3 response at 30°N (left column of plots) and DE2 response at 30°S (right column of plots), i.e. at these modip latitudes where the response is maximum. The main feature of the altitude structure at both responses is that there are upper level response (above ∼300 km height) and bottom level response (below ∼250 km height). The two regions of enhanced response are separated by a narrow altitude zone where the response is almost absent. The upper level response at ±30° modip latitude has maximum near 400–450 km height while the bottom level one near ∼200–250 km. In the NH the upper and bottom level DE3 responses are similar while in the SH the upper level DE2 response is stronger than the bottom level one.

Fig. 5 Altitude structure of the amplitudes in MHz (*upper row* of plots) and phases in degrees (*bottom row* of plots) of the electron density DE3 response at 30°N (*left column* of plots) and DE2 response at 30°S (*right column* of plots); the *black arrows* at the bottom part of the phase plots display the vertical phase structure

The phase structures at both altitude regions are very different: while in the upper level response there is no any vertical phase structure in the bottom level there is such structure. The latter is well evident near the altitudes of enhanced response and is marked by black arrows in the bottom parts of the two phase plots. The absence of vertical phase structure in the upper level response indicates that the response is shaped mainly by the vertical plasma drift. The direct effect by the tides cannot be excluded also as the wind/temperature tides are almost trapped at these heights. The vertical phase structure in the bottom level response revealed upward propagation of the response on the average above 150–180 km altitude.

The above described important feature of the ionospheric response to nonmigrating tides forced from below, reported for the first time by Mukhtarov and Pancheva (2011), can be illustrated better in altitude-longitude frame. The upper plot of Fig. 6 shows the altitude-longitude structure of the monthly mean electron density DE3 variability in MHz at modip 30°N for September 2008 while the bottom plot shows the monthly mean DE2 variability at 30°S for January 2008; both electron density variabilities are at 00 UT. This type of presentation clearly distinguishes the two different types of response: the upper level response composed of trapped oscillations and bottom level response consisting of propagating oscillations. Generally, above ∼175 km altitude the slope of the bottom level response is eastward (as the DE3 and DE2 are zonally eastward propagating tides) which indicates an vertical upward propagation. The observed propagating tidal response at ±30° modip latitudes is a signature for a possible direct tidal effect in the considered altitude region. The tropical response has maximum near ∼200–230 km altitude. This could be an indication for a possible effect of the vertical wind DE3 tide (Oberheide et al. 2009), or a response shaped by a DE3/DE2 meridional wind modulated Pedersen currents. There is also
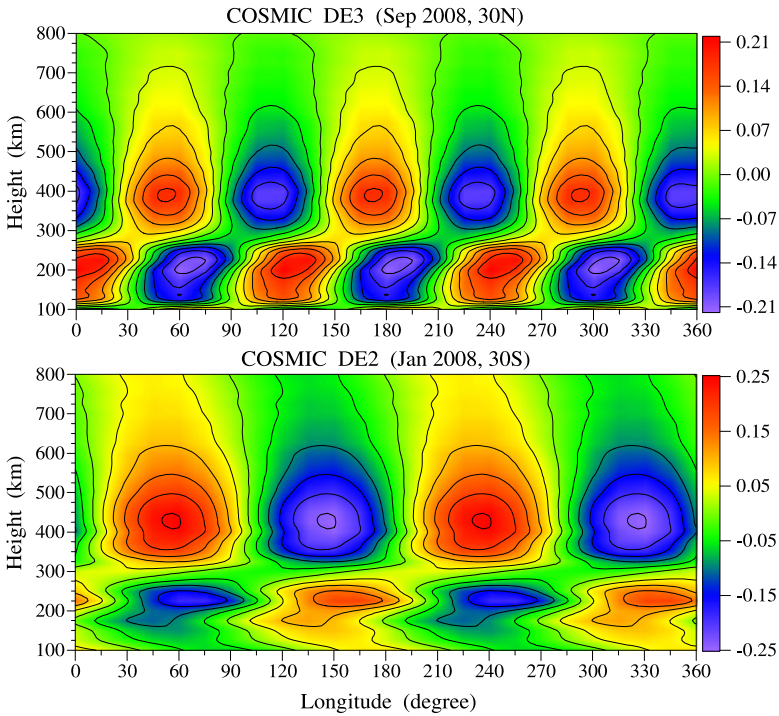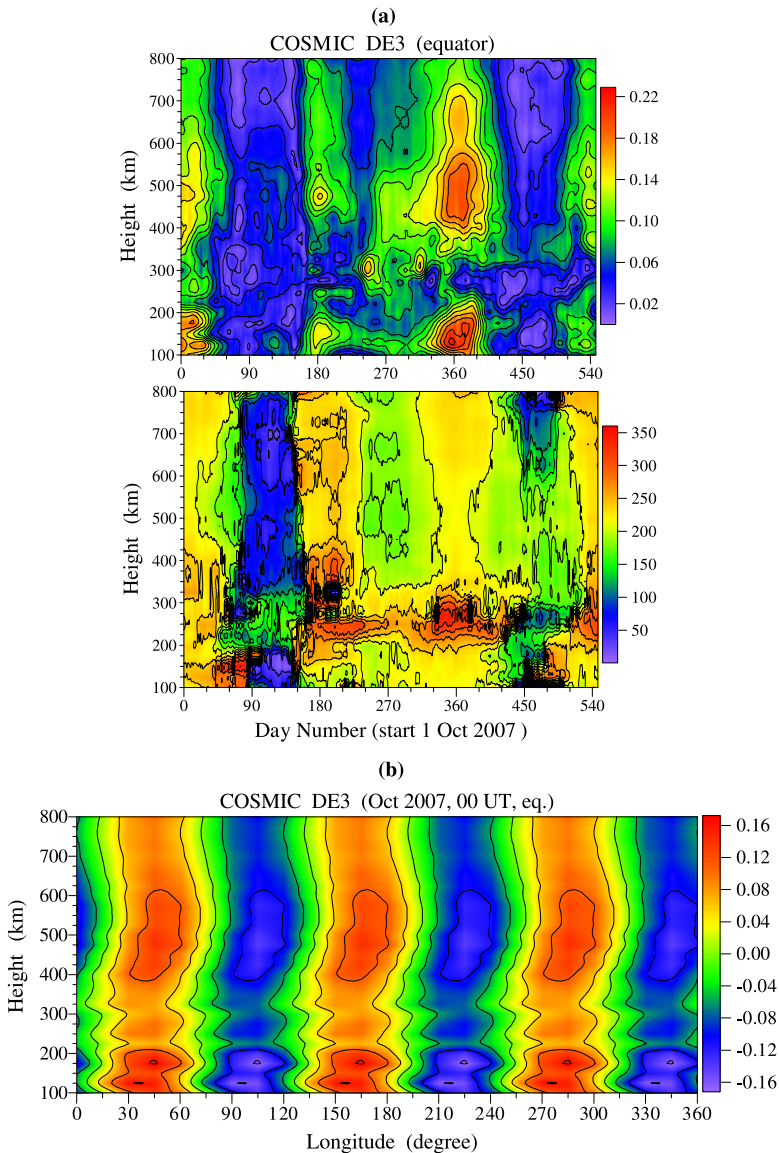
Fig. 6 Altitude-longitude structure of the electron density DE3 variability at 30°N in September 2008 (*upper plot*) and DE2 variability at 30°S in January 2008 (*bottom plot*); both plots present the tidal variability at 00 UT

a possibility of coupling between tides and the ionosphere via changes in neutral density and particularly a modification of [O], i.e. [O]/[N$_2$], which has effect on the recombination rate.

Figure 7a presents the electron density DE3 response over the equator; the amplitudes in MHz are shown in the upper plot while the phases in degrees can be seen in the bottom plot. There are also two altitude regions of enhanced response: the upper level response that is expanded from ∼400 km up to ∼700 km height (particularly that in September/October) and the bottom level one that maximizes near and below 150 km height. In this case however the phases at both regions are the same (particularly where the amplitudes are large and the phases can be defined with a high degree of confidence). Figure 7b displays the altitude-longitude structure of the monthly mean DE3 electron density variability over the equator for October 2007 at 00 UT. In this case the upper level and bottom level responses are in phase. Very recently Brahmanandam et al. (2011) have considered vertical and longitudinal electron density structures of the equatorial E- and F-regions in September–November 2007 and found very similar picture as that shown in Fig. 7b. The authors used also COSMIC electron density data but analyzed them in the traditional fixed LT frame (i.e. four structures are seen) by subtracting the background value from the original data. The obtaining of similar results by using two very different data analysis methods is a quite encouraging support of the result shown in Fig. 7b.

Figure 8 presents the latitude-altitude cross sections of the electron density DE3 response on September 26, 2008 (left plot) and DE2 response on March 25, 2008 (right plot), e.g.

Fig. 7 (**a**) Altitude structure of the amplitude in MHz (*upper plot*) and phase in degrees (*bottom plot*) of the electron density DE3 response over the equator; (**b**) Altitude-longitude structure of the electron density DE3 variability over the equator in October 2007 at 00 UT

when the responses are strong (see Fig. 5). The both upper level responses clearly indicate the influence of the "fountain effect". Nevertheless that we consider equinoctial months the responses are stronger in the Southern Hemisphere (SH). It is worth noting that during the entire considered period of time (October 2007–March 2009) the ionospheric DE3 and DE2 responses at altitude of 400 km are stronger in the SH (see Fig. 4, 400 km height). This could be due to some equinoctial asymmetry of the vertical plasma drift found recently by
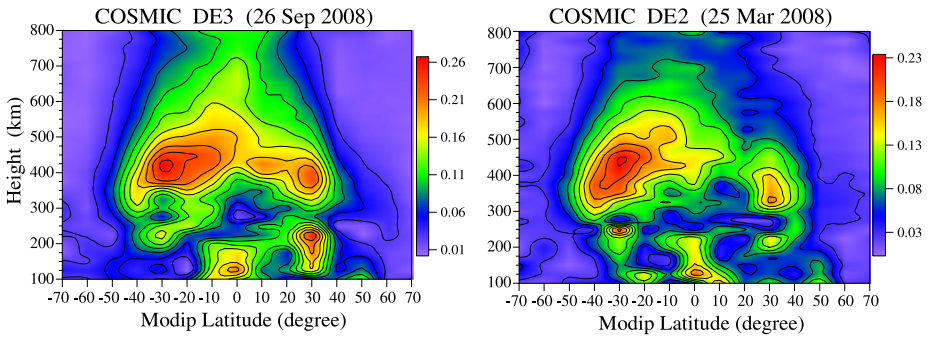
Fig. 8 Altitude-latitude structures of the electron density DE3 and DE2 responses observed on September 26, 2008 and March 25, 2008 respectively

Ren et al. (2011). The DE3 and DE2 bottom level responses are composed of two parts: a tropical response, near ±30° modip latitude, and over the dip equator. While the tropical response maximizes near 200–230 km height that over the equator amplifies at lower thermosphere, near 130–150 km. It should be noted that the bottom level tropical responses are just underneath the upper level ones.

It seems from Fig. 8 that the upper level DE3/DE2 response is shaped mainly by the DE3/DE2 modulated vertical plasma drifts. This is borne out by the strong DE3/DE2 h_mF2 response shown in Fig. 1 which reaches amplitudes of ∼9 km.

England et al. (2010) found however that in addition to the E-region dynamo modulation other effects have the potential to contribute to the coupling between tides and the F-region ionosphere: neutral density variations, changes in thermospheric [O]/[N$_2$] ration, and meridional winds at F-region altitudes. In order to assess if these alternative effects contribute to the ionospheric DE3/DE2 response above ∼300 km altitude we analyze both bottom and top slope coefficients described by (1), but our interest is directed mainly to the result for the top slope coefficient. We remind that these coefficients represent the bottom- and top-side vertical gradients of the electron density profile.

Figure 9 shows the DE3 (left column of plots) and DE2 (right column of plots) response in the top (upper row of plots) and bottom (bottom row of plots) slope coefficients. It is seen that both coefficients display clear response at the same time when the response is seen in the electron density (Figs. 4 and 5) and in h_mF2 (Fig. 2). The observed DE3 and DE2 variations have quite large amplitudes being near 10% of their mean values. This means that both (bottom- and top-side) slopes of the electron density profiles change during the coupling between tides and the ionosphere. This is an indication that the above mentioned additional affects contribute not only to shaping the bottom level response but to the upper level one as well.

The above obtained main features of the ionospheric DE3/DE2 response are seen in all nonmigrating responses considered in this study, i.e. nonmigrating diurnal, semidiurnal and terdiurnal tidal responses with zonal wavenumber up to 4. The SPWs with zonal wavenumber up to 4 are also considered in this study (see the third term on the right hand side of (2)). In general, the main features of the ionospheric SPW variability are similar to those of the tidal response, but the influence of the "fountain effect" in some cases is significantly weaker.
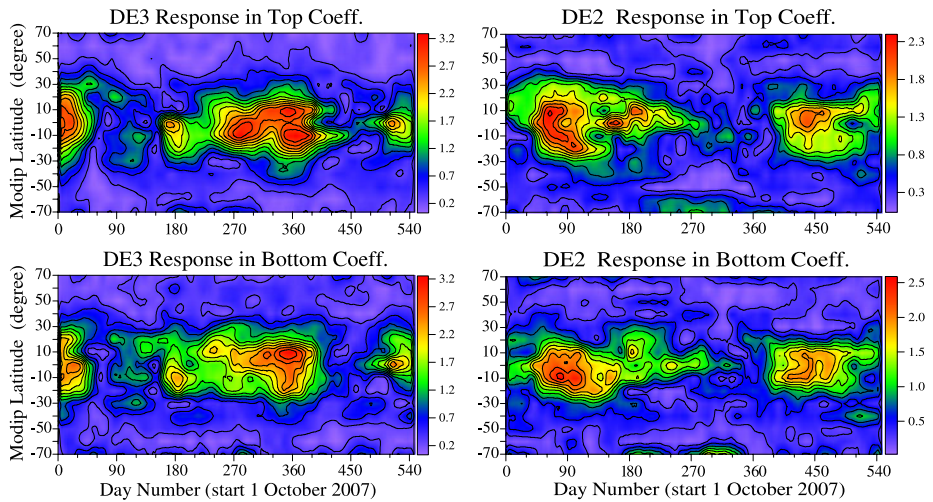
Fig. 9 Latitude-time cross sections of the DE3 (*left column* of plots) and DE2 (*right column* of plots) responses seen in the top (*upper row* of plots) and bottom (*bottom row* of plots) slope coefficients defining the electron density profiles

4 Contributors to the WN4 and WN3 Longitude Structures

It has been already mentioned that the WN4 longitude structure is the most prominent pattern observed by quasi-sun-synchronous satellites in a variety of ionospheric and thermospheric parameters. This structure has been often attributed to the DE3 tide based usually on the annual and LT variations of the WN4 structure. We noted also that all observational reports mentioned in the Introduction part were studied in a fixed LT. Hence, the observed structure cannot be directly related to a certain tidal component. Our approach however allows assessing the possible contributions of all waves that can force the WN4/WN3 structures and this is a significant advantage of the used in this study data analysis method.

As we noted before if only the diurnal and semidiurnal tides are considered, the WN4 structure can be forced by: DE3, DW5, SW6, SE2 and SPW4. The wave components with zonal wavenumber larger than 4 are not included in the decomposition procedure of both SABER and COSMIC data (see the formula (2)) hence the contribution of the DW5 and SW6 tides cannot be estimated. In general, the tidal components with high zonal wavenumbers have short vertical wavelengths hence they are more sensitive to the increasing dissipation in the lower thermosphere, i.e. they are susceptible to dissipation.

The climatology of the SABER eastward nonmigrating tides has been studied by Pancheva et al. (2010b) and found that the SE2 tide is one of the strongest semidiurnal nonmigrating tides with coherent latitude and altitude structures. It amplifies near tropics (±30°) and reaches amplitudes of ∼7 K in the E-region of ionosphere (at ∼115 km altitude). The SE2 tide, particularly that in the NH, when propagating upward it propagates toward the equator as well. During the time period under consideration, the SABER SE2 tide shows some amplification in March and September–October 2008 with amplitudes of ∼5–5.5 K (not shown here). This tide is excited by latent heat release in the tropical troposphere, with some contributions from net radiative heating (Zhang et al. 2010). It can be produced also by a nonlinear interaction between the DE3 and migrating diurnal tide (DW1) tides (Hagan et al. 2009). The SE2 tide has relatively short vertical wavelength in winter,

~30 km, but longer one in summer and equinoxes, ~40–45 km, i.e. it might be efficient in the E-region dynamo modulation during the time when the ionospheric WN4 structure is observed.

The SABER SPW4 has relatively small amplitudes (~2.5–2.8 K) in the lower thermosphere over the equator in August–October 2008 (not shown here). However, very recently Oberheide et al. (2011) has reported quite large zonal wind SPW4 (~12 m/sec) with long vertical wavelength seen in the TIDI measurements over the equator (see Fig. 13 from Oberheide et al. 2011). This result fits well into recent model results presented by Hagan et al. (2009) where it is found that the SPW4 is excited by nonlinear interaction between the DE3 and the migrating diurnal tide (DW1). The observed strong zonal wind SPW4 with long vertical wavelength over the equatorial E-region indicates that this wave might efficiently modulate the E-region dynamo.

Figure 10 shows the latitude structure (±70°) of the amplitudes in MHz of the electron density DE3 (upper plot), SPW4 (middle plot) and SE2 (bottom plot) responses at altitude of 400 km. To facilitate the comparison the scales at all plots are the same. It is evident right away that the DE3 and SPW4 responses have very similar seasonal behaviour and similar amplitudes at 400 km height; while the largest amplitude of the DE3 response is ~0.30 MHz that of the SPW4 is 0.29 MHz. As it has been expected the SE2 response is much weaker, ~0.16 MHz. Similarly to the DE3 and SPW4 waves the SE2 response shows also amplification in July–October 2008.

If the wave responses seen in Fig. 10 contribute to the WN4 structure (seen in a LT fixed frame) then the ionospheric variability forced by the superposition of the DE3, SPW4 and SE2 waves should be similar to that of the DE3 tide alone, i.e. the superposition has to have similar seasonal behaviour and the same longitudinal structure as the DE3 tide. If each wave has a seasonal variability similar to that of the DE3, as it was shown in Fig. 10, then this will be valid for the superposition as well. Figure 11 presents the altitude-longitude structure of the electron density DE3 (upper plot) and the superposition of DE3, SE2 and SPW4 (bottom plot) variability at 30°S in October 2008 at 00 UT. The comparison between the two electron density variabilities reveals high degree of similarity: (i) the same longitude structure; (ii) two different types of response; while the upper level response is composed of trapped oscillations and bottom level one consists of propagating oscillations, and (iii) the longitude maxima of both upper and bottom level responses are situated at almost the same longitudes. There is however one important difference; while the maximum amplitude of the DE3 response in October 2008 is 0.27 MHz that of the superposition is ~0.5 MHz, i.e. almost two times stronger. This is very important fact that explains why the WN4 structure can be distinguished sometimes even in the raw data.

As we mentioned before the ionospheric WN3 structure can be forced by: DW4, DE2, SW5, SE1 and SPW3. All these waves, except the nonmigrating SW5 tide, are included in the decomposition scheme of SABER and COSMIC data and their contribution to the WN3 structure can be assessed. The analysis of the SABER temperatures revealed that the SW4, SE1 and SPW3 have amplitudes of ~5–6 K in the equatorial E-region of the ionosphere (~110–115 km altitude) and that they amplify usually in winter (not shown here). This result supports their contribution to the WN3 structure which is observed mainly in winter. The SPW3 penetrates to the lower thermosphere from below; it has stratospheric and mesospheric amplifications at altitudes of ~45 km and 85–90 km respectively. It might be the most efficient wave among the above mentioned ones in modulating the E-region dynamo because of having comparatively long vertical wavelength.
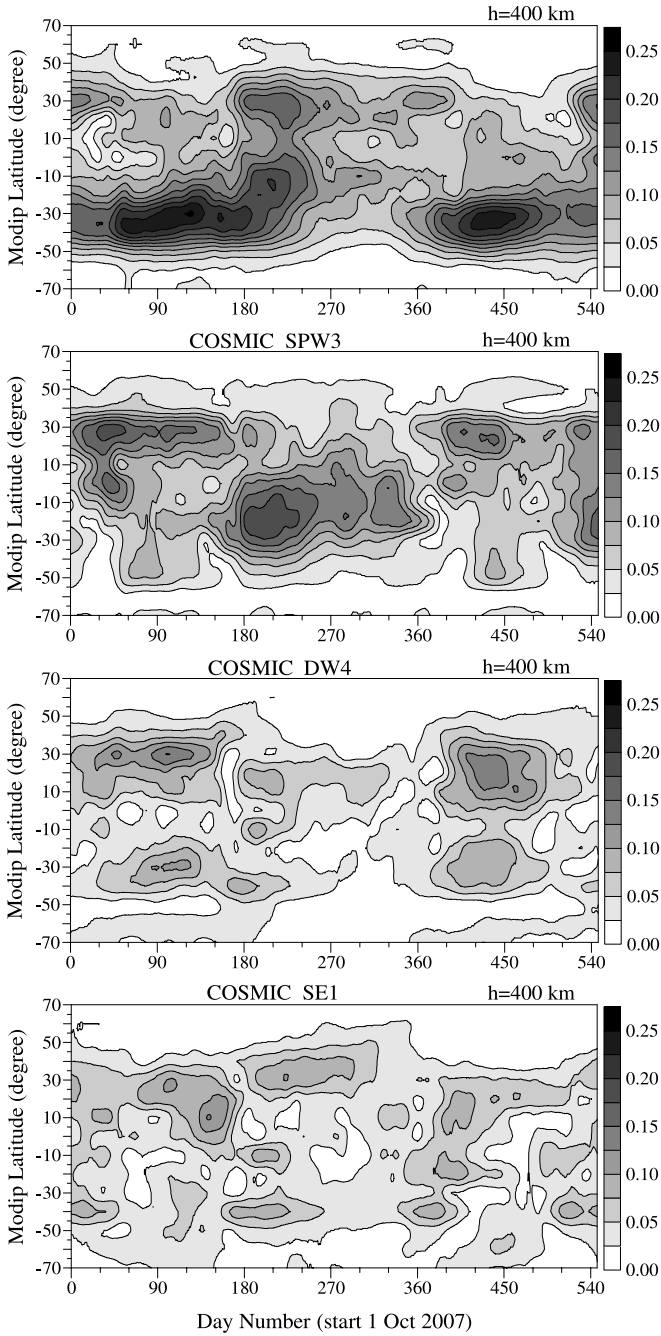
Figure 12 displays the latitude structure (±70°) of the amplitudes in MHz of the electron density DE2 (upper plot), SPW3 (second from above plot), DW4 (third from above plot)
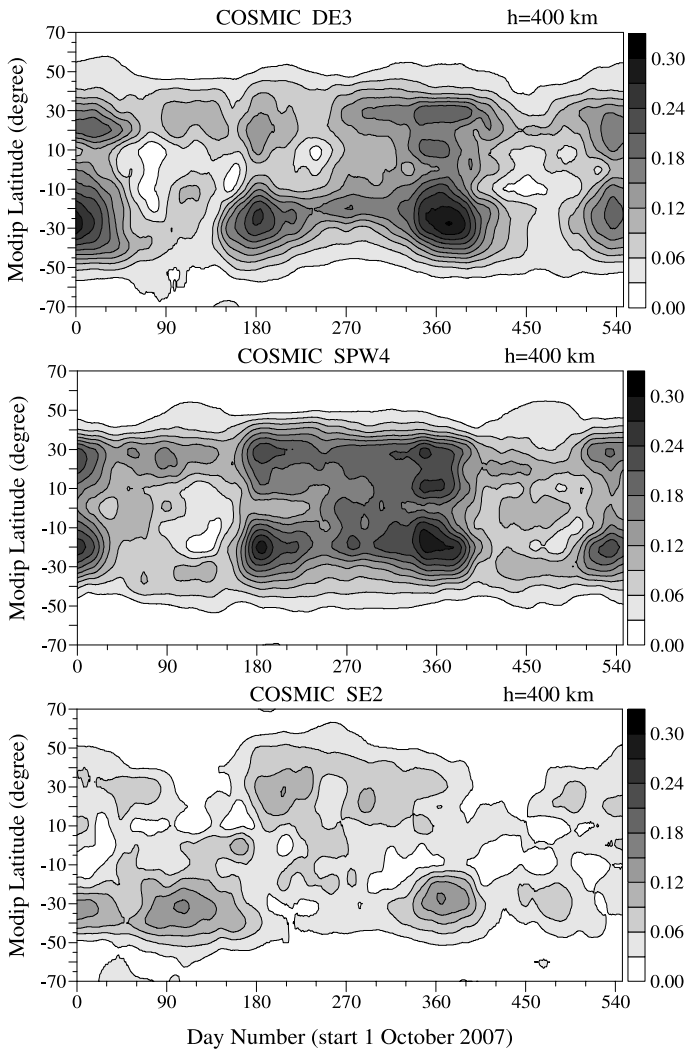
Fig. 10 Latitude structure ($\pm 70°$) of the amplitudes in MHz of the electron density DE3 (*upper plot*), SPW4 (*middle plot*) and SE2 (*bottom plot*) responses at altitude of 400 km; the scales at all plots are the same

and SE1 (bottom plot) responses at altitude of 400 km. Again to facilitate the comparison the scales at all plots are the same. The vertical arrangement of the ionospheric responses is based also on their amplitudes as the strongest response is shown on the uppermost plot, i.e. DE2 response which is ~ 0.25 MHz. Next to the DE2 are as follows: SPW3 (~ 0.20 MHz), DW4 (~ 0.15 MHz) and SE1 (~ 0.13 MHz) responses. It is evident also that all these responses amplify during winter and spring, i.e. when the WN3 structure is often observed.

Figure 13 display the altitude-longitude structure of the electron density DE2 (upper plot) and the superposition of DE2, DW4, SE1 and SPW3 (bottom plot) variability at 30°S in January 2008 at 00 UT. Again the comparison between the both responses indicates high degree of similarity. All details valid for the comparison shown in Fig. 11 are applicable in
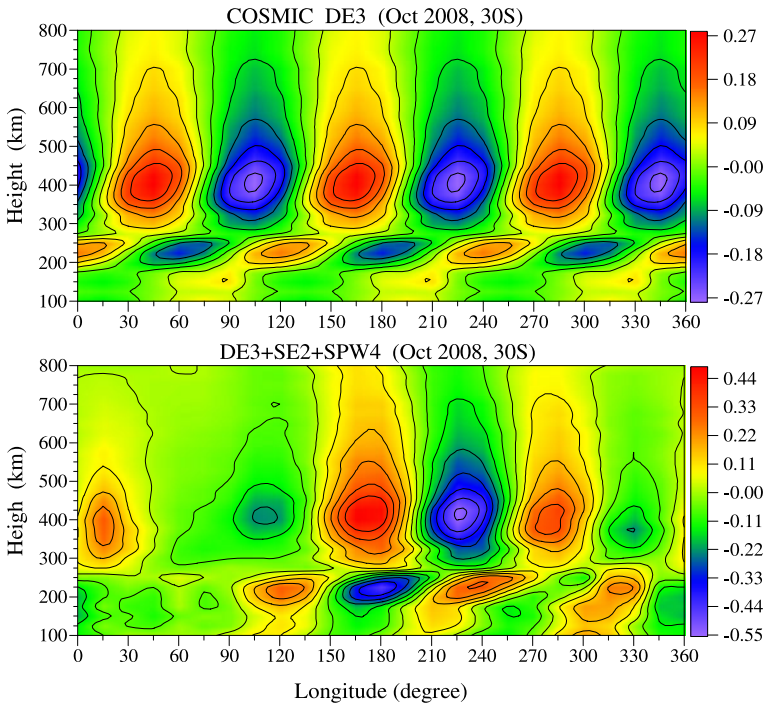
Fig. 11 Altitude-longitude structure of the electron density DE3 (*upper plot*) and the superposition of DE3, SE2 and SPW4 (*bottom plot*) variability at 30°S in October 2008 at 00 UT

this case as well. Here also the superposition response of ∼0.36 MHz is 1.5 time stronger than the DE2 response (∼0.25 MHz).

The results of this part are obtained for the first time from an analysis of the COSMIC electron density measurements where all forced from below waves are extracted simultaneously from the data. These new experimental results give an explanation why the WN4 and partly WN3 longitude structures are so prominent pattern in the ionosphere. We present experimental evidence which indicate that the WN4 (WN3) structure is not generated only by the DE3 (DE2) tide as it has been often assumed. The DE3 (DE2) tide remains the leading contributor, but the SPW4 and SE2 (SPW3, DW4 and SE1) waves have their effects as well in a way that the ionospheric response becomes almost double (1.5 time stronger).

5 Electron Density Sun-Synchronous 24-, 12- and 8-h Tidal Responses

We mentioned before that the sun-synchronous 24-h (DW1), 12-h (SW2) and 8-h (TW3) electron density oscillations are produced by a combination of the diurnal variability of the photo ionization which depends on the solar zenith angle and the effect of the migrating diurnal, semidiurnal and terdiurnal tides forced from below. It was mentioned also that the data analysis method used in this study cannot separate the two effects. Having in mind the main features of the latitude and altitude structures of the electron density tidal response described in Part 3, we will make an attempt to assess the effect of the migrating tides on the DW1, SW2 and TE3 electron density oscillations separated from the COSMIC data.

Fig. 12 Latitude structure (±70°) of the amplitudes in MHz of the electron density DE2 (*upper plot*), SPW3 (*second from above plot*), DW4 (*third from above plot*) and SE1 (*bottom plot*) responses at altitude of 400 km; the scales at all plots are the same
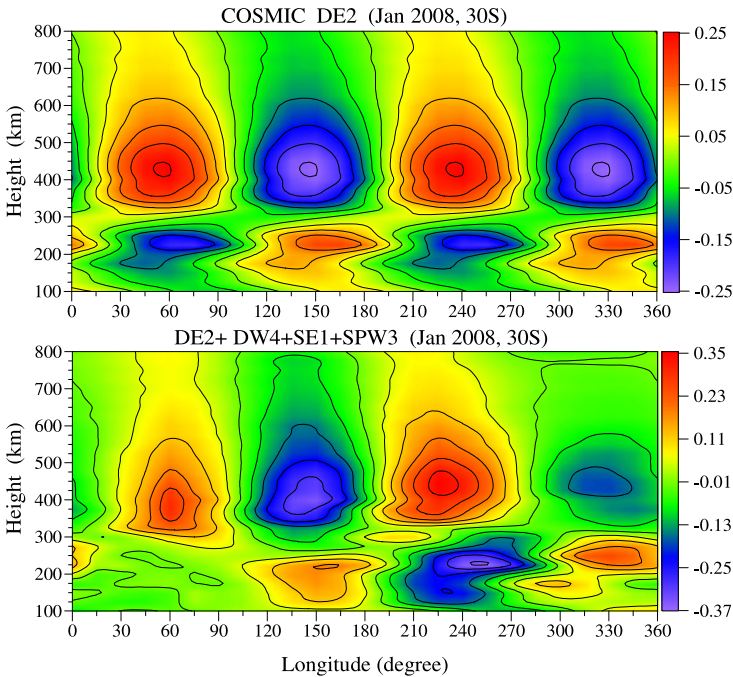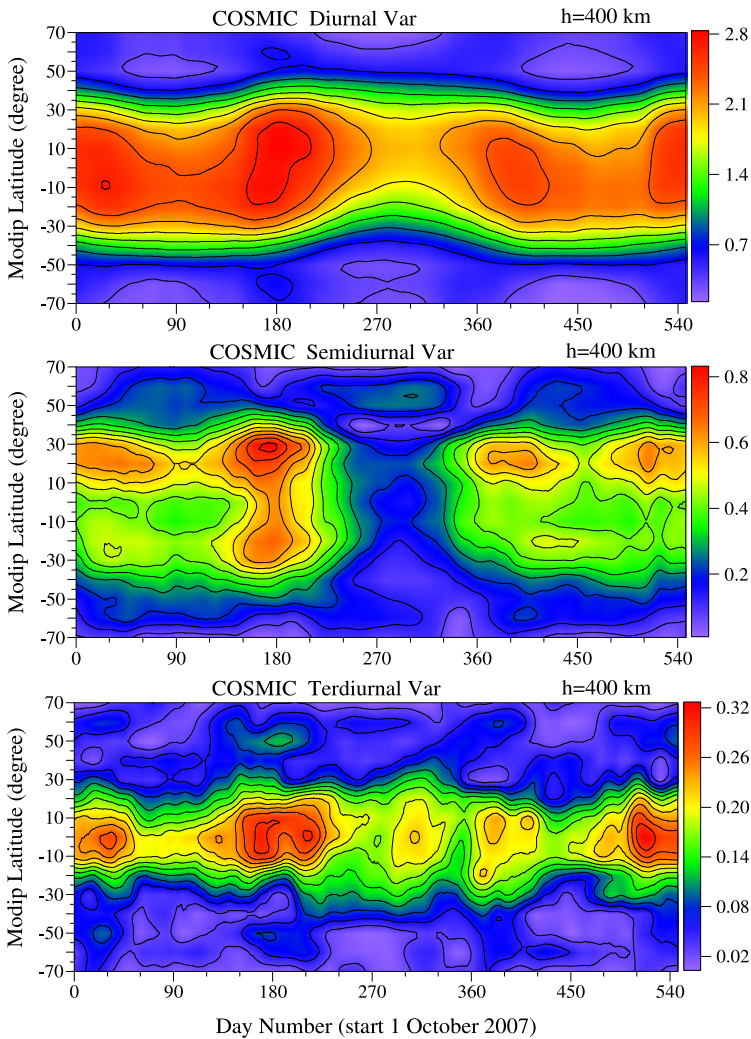
Fig. 13 Altitude-longitude structure of the electron density DE2 (*upper plot*) and the superposition of DE2, DW4, SE1 and SPW3 (*bottom plot*) variability at 30°S in January 2008 at 00 UT

Figure 14 shows the latitudinal structures of the sun-synchronous diurnal (upper plot), semidiurnal (middle plot) and terdiurnal (bottom plot) oscillations observed in the COSMIC electron density at 400 km height. We display the results at 400 km height because the splitting around the equator of the DE3 and DE2 electron density responses (Fig. 4) was most clearly evident at the height of 400 km. While the semidiurnal oscillation shows clear splitting around the equator with maxima near ±20–30° modip latitude the diurnal and terdiurnal ones does not show such splitting. It is worth noting that the used in this study a latitude resolution of 10° could screen some fine splitting located close to the equator (not far away from ±10°). As the latitude structure of the nonmigrating tidal responses clearly revealed maxima locations near ±30°, hence the latitude resolution of 10° is enough for the basic aims of this study.

Figure 15a presents the altitude structure of the sun-synchronous diurnal oscillation; the upper plot shows the amplitude in MHz, while the bottom plot shows the phase in degrees. There isn't any signature of the two altitude regions of ionospheric response which is typical for the nonmigrating tidal effect. The latitude (upper plot of Fig. 14) and altitude (Fig. 15a) structures of the COSMIC sun-synchronous 24-h electron density oscillation indicate that this response is shaped mainly by the photo ionization, i.e. it is due to a solar zenith angle effect. Figure 15b displays the altitude-longitude structure of the electron density DW1 variability over the equator in March 2008 at 00 UT. The maximum diurnal variability in March is seen at ∼350 km height and the minimum electron density is seen between 02 and 03 am; the latter is supported by numerous ground-based ionosonde measurements.

Figure 16a presents the altitude structure of the sun-synchronous 12-h oscillation at latitude of 30°N (left column of plots) and 30°S (right column of plots); again the result for

Fig. 14 Latitude structure (±70°) of the amplitudes in MHz of the electron density DW1 (*upper plot*), SW2 (*middle plot*) and TW3 (*bottom plot*) responses at altitude of 400 km

the amplitude is shown in the upper row of plots while for the phase is in the bottom row of plots. In this case the two altitude regions of response, separated by a narrow zone with no response, are clearly outlined. The SW2 amplitude particularly at the NH tropic reaches ∼0.9 MHz, as the SW2 maxima are situated near 350–400 km height. We remind that the SABER SW2 tide also maximizes at tropical lower thermosphere. The difference in the phase structure at the tropics is also well evident: no vertical phase structure in the upper level and the presence of phase structure at the bottom level; the latter is marked by the red arrows situated in the bottom side of the phase plots. The vertical phase structure indicates that the bottom level response at least above ∼150 km height is vertically upward propagating response.
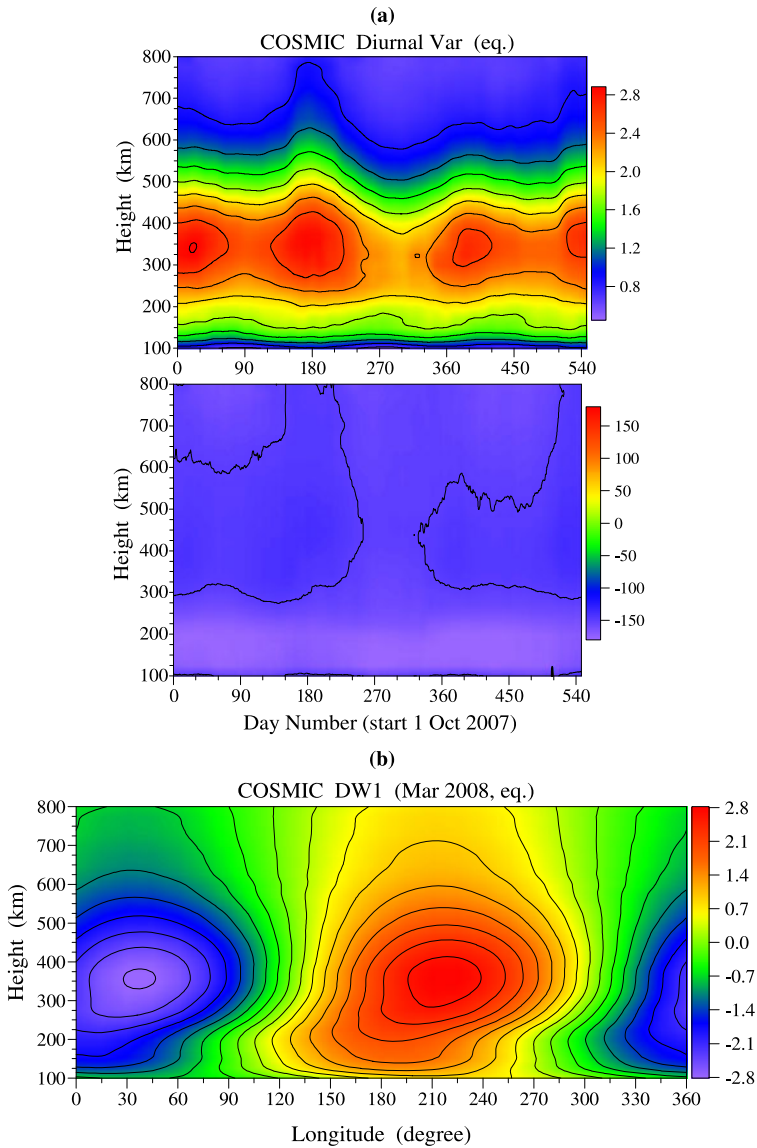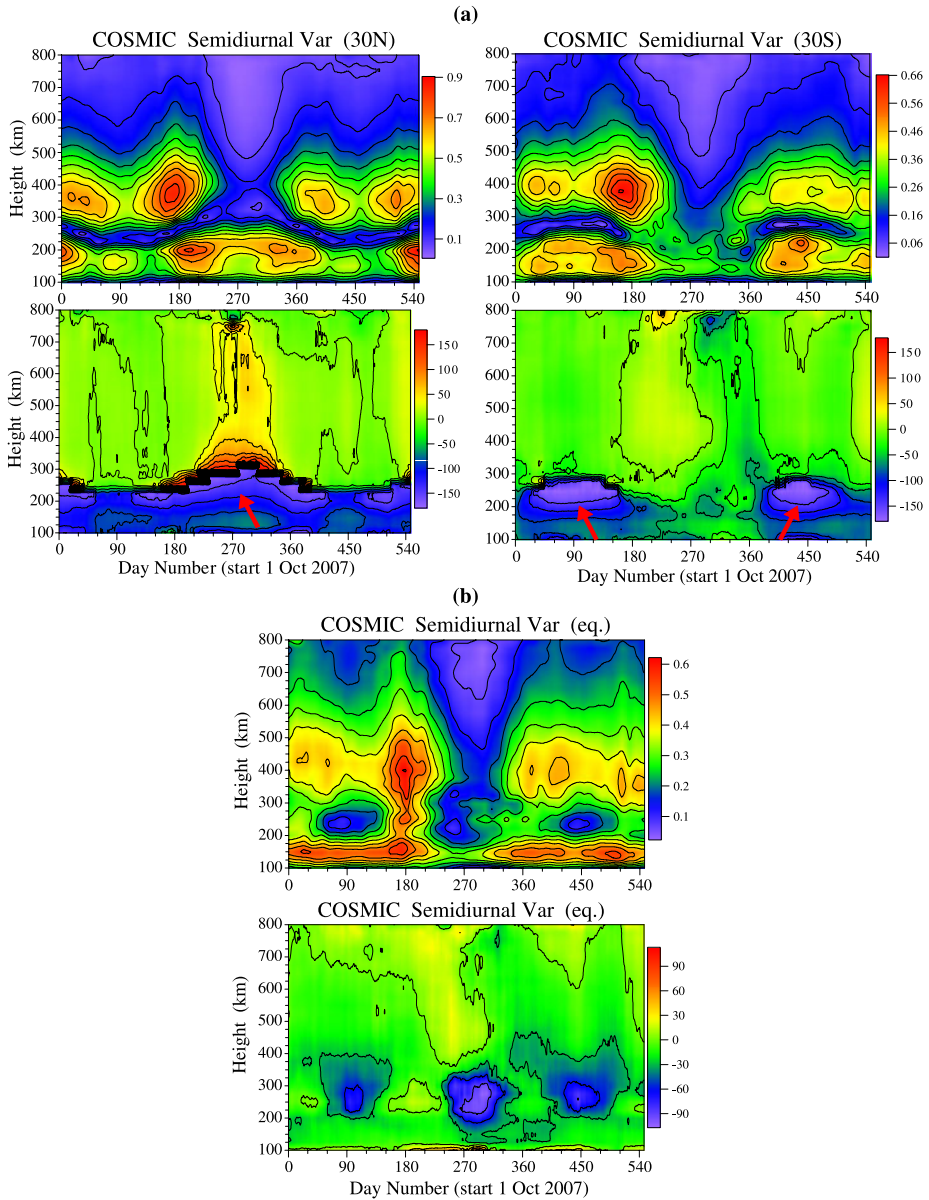
Fig. 15 (**a**) Altitude structure of the amplitude in MHz (*upper plot*) and phase in degrees (*bottom plot*) of the electron density DW1 response over the equator; (**b**) Altitude-longitude structure of the electron density DW1 variability over the equator in March 2008 at 00 UT

Figure 16b is the same as Fig. 16a, but for the SW2 response over the equator. Two levels of response are again clearly distinguished. Similarly to the DE3 response over the equator, shown in Fig. 7a, there is also no phase difference between the upper and bottom level phase structures. The SW2 response over the equator is weaker than those at the tropics and it reaches ∼0.6 MHz.

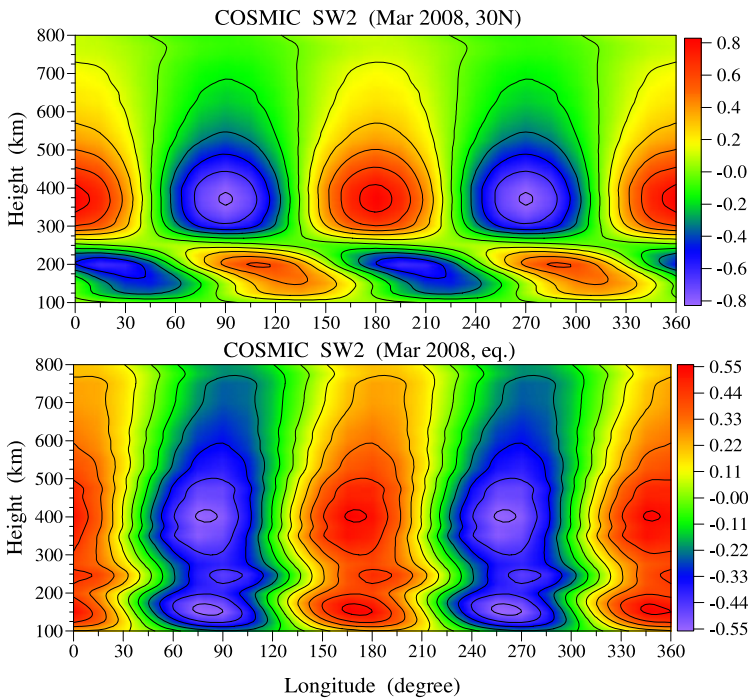Figure 17 presents the altitude-longitude structure of the electron density SW2 variability at 30°N (upper plot) and over the equator (bottom plot) in March 2008 at 00 UT. The SW2

Fig. 16 (**a**) Altitude structure of the amplitudes in MHz (*upper row* of plots) and phases in degrees (*bottom row* of plots) of the electron density DW1 responses at 30°N (*left column* of plots) and at 30°S (*right column* of plots); the *red arrows* at the bottom part of the phase plots display the vertical phase structure; (**b**) The same as (**a**) but over the equator

response at tropics is similar to the tropical DE3/DE2 response shown in Fig. 6. The upper level response is composed of trapped oscillations and bottom level response consists of propagating oscillations. Generally, above ∼150 km altitude the slope of the bottom level response is westward (as the SW2 is zonally westward propagating tide) which indicates a
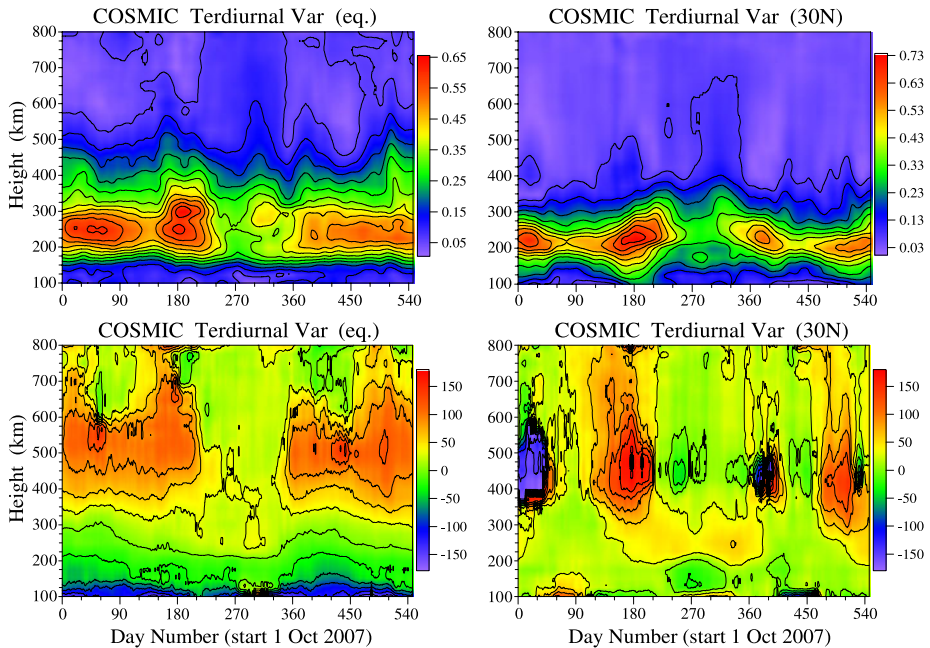
Fig. 17 Altitude-longitude structure of the electron density SW2 variability at 30°N (*upper plot*) and over the equator (*bottom plot*) in March 2008 at 00 UT

vertical upward propagation. The SW2 response over the equator (bottom plot) is similar to the equatorial DE3 response shown in Fig. 7b with no vertical phase structure in the entire altitude range.

The latitude (middle plot of Fig. 14) and altitude (Figs. 16 and 17) structures of the COSMIC sun-synchronous 12-h electron density oscillation indicate that this ionospheric oscillation is significantly affected by the migrating SW2 tide forced from below. We note that the climatology of the SABER SW2 tide (Pancheva et al. 2009b) revealed that this is the strongest semidiurnal tide observed in the low-latitude E-region of the ionosphere. The SW2 vertical wavelength increases during the equinoctial and summer months, hence its efficiency for electric field generation increases as well.

Figure 18 shows the altitude structure of the amplitudes in MHz (upper row of plots) and phases in degrees (bottom row of plots) of the electron density TW3 responses over the equator (left column of plots) and at 30°N (right column of plots). This ionospheric oscillation, similarly to the DW1 one, does not show two altitude levels of response. The largest TW3 response over the equator is near 250 km altitude, while at the tropics it is slightly lower, ~225 km. The response maximizes during the equinoxes, similarly to the SABER TW3 tide. The TW3 amplitude at the tropic is slightly larger than that over the equator, 0.73 MHz vs. 0.65 MHz. In general, the ionospheric TW3 response is very strong and it approaches the SW2 response. The TW3 phase structure is completely different from those of the DW1 and SW2 responses. At both latitudes there is an altitude region with a phase maximum; such region above the equator is located near 500–550 km while at 30°N it is near 400–450 km. The phase plots reveal also that below and above this region the phase decreases, i.e. there is upward/downward phase progression in electron density perturbation. This is an indication
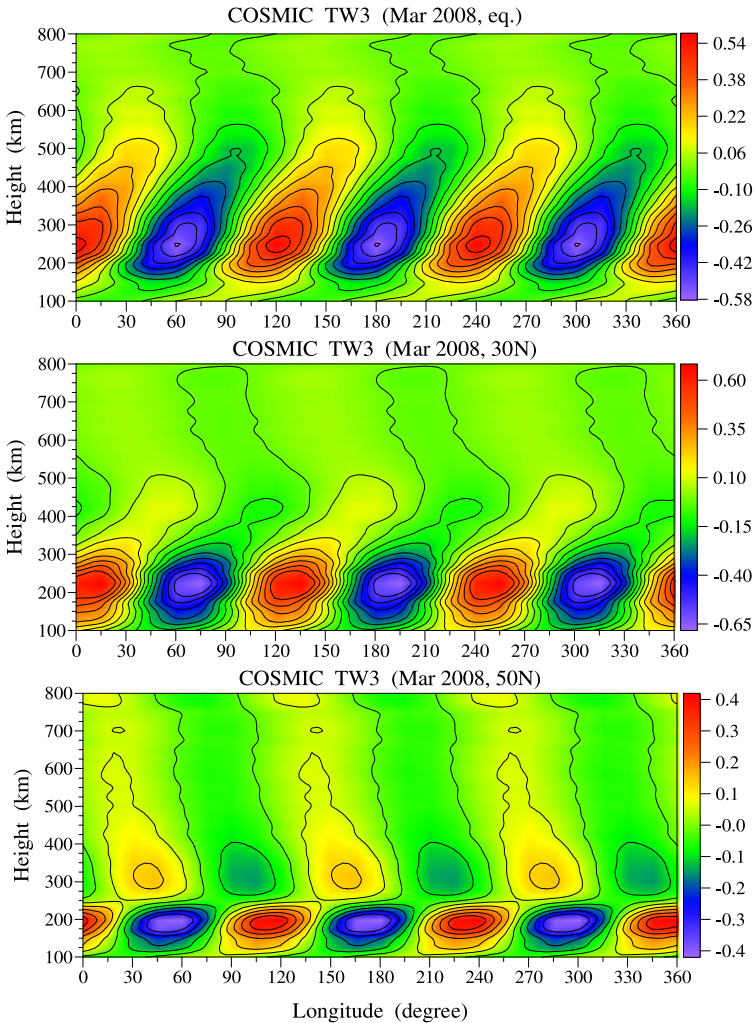
Fig. 18 Altitude structure of the amplitudes in MHz (*upper row* of plots) and phases in degrees (*bottom row* of plots) of the electron density TW3 responses over the equator (*left column* of plots) and at 30°N (*right column* of plots)

that the electron density TW3 response propagates downward/upward below and above the phase maximum region (i.e. there is downward/upward energy propagation).

The above described peculiar feature of the ionospheric TW3 response is illustrated better in the altitude-longitude frame. Figure 19 displays the altitude-longitude structure of the electron density TW3 variability over the equator (upper plot), at 30°N (middle plot) and at 50°N (bottom plot) in March 2008 at 00 UT. The main features of the TW3 response can be summarized as: (i) at all modip latitudes the slope of the largest oscillations is eastward, this indicates an downward propagation of the oscillations; (ii) there is lowering of the altitude with the largest response when the modip latitude increases; it is near 250 km over the equator while is near and even below 200 km at 50°N; (iii) the lowering of the altitude with the largest response is accompanied by a lowering of the altitude where the phase slope changes its direction. It is worth noting that the standard version of the TIME-GCM model (i.e. version where only the migrating tides from the GSWM are included) also produces downward/upward phase progression in the electron density TW3 perturbation at geographic latitude of 31°N (which is ∼40–50°N modip latitude), i.e. the electron density TW3 response does not correspond to the neutral wind and temperature TW3 upward energy propagation in the lower-middle thermosphere (up to ∼300 km altitude) (H.-L. Liu, personal communication, 2011).

The peculiar vertical structure of the ionospheric TW3 response hints at possible coupling between the SW2 tide forced from below and the diurnal variability of the electron density, i.e. at ion-neutral momentum coupling. The answer of this question cannot be found only from the analysis of COSMIC data; it needs further detailed numerical simulations as well.

Fig. 19 Altitude-longitude structure of the electron density TW3 variability over the equator (*upper plot*), at 30°N (*middle plot*) and at 50°N (*bottom plot*) in March 2008 at 00 UT

6 Summary and Concluding Comments

The paper is an overview of the ionospheric response to atmospheric tides forced from below. Most of the results have been very recently produced and they provide strong observational support for tidal-ionosphere coupling processes beyond the lower thermosphere dynamo region. Moreover, not traditional data concerning of middle atmosphere and ionosphere but modern satellite-board data (COSMIC and SABER/TIMED) were effectively used for the analysis. The tidal waves from the two data sets have been extracted by the same data analysis method described in detail by Pancheva et al. (2009a). The similarity between the lower thermospheric temperature tides and their ionospheric electron density responses provides evidence for confirming the new paradigm of atmosphere-ionosphere coupling.

It was mentioned in the COSMIC data section that the electron density profiles employed in this study were retrieved by using a RO inversion technique. The electron density profiles obtained by this technique have been validated by comparing them with ground-based ionosonde and Incoherent Scatter Radar (ISR) observations (Lei et al. 2007; Kelley et al. 2009). The RO inversion approach relies on a few assumptions and approximations described in detail by Kuo et al. (2004) and Lei et al. (2007). All of them introduce some limitations and possible errors in determining the electron density profiles. Recently it has been found that particularly the spherical symmetry assumption used in Abel inversion is possibly the most significant error source (Schreiner et al. 1999; Lei et al. 2007; Kelley et al. 2009; Yue et al. 2010). In Yue et al. (2010) and Liu et al. (2010) an attempt has been made to simulate error distribution of RO electron density profiles from the Abel inversion by using some empirical ionospheric models. Their results show that the retrieved N_mF2 and h_mF2 are generally in good agreement with the true values, but the reliability of the retrieved electron density degrades at low latitudes and altitudes. Specifically the above mentioned authors found that the Abel retrieval method introduces artificial plasma caves underneath the EIA crests along with three density enhancements in adjacent latitudes. The artifact appears mainly below 250 km altitudes and becomes pronounced when the EIA is well developed. Liu et al. (2010) found also that the deviation of the retrieved electron density from the true one depends also on the local times.

The above mentioned simulations indicate that the error in defining the electron density below 250 km height depends on the latitudes where the EIA crests are located. In our case the EIA crests can be defined by the latitude structures of the electron density mean value (the first and second terms on the right hand side of (2) which is not used in this paper) and the sun-synchronized ionospheric tidal responses (DW1, SW2 and TW3). In general, the latitude maxima (i.e. EIA), obtained by the superposition of the above mentioned components, are situated near $\pm 30°$ modip latitude (not shown here). We remind that the upper level COSMIC nonmigrating electron density responses were located also near $\pm 30°$ modip latitude and that the bottom level responses are just underneath the upper level ones. This means that the bottom level responses are just underneath the EIA crests. We remind also that the bottom level response at tropics has vertically propagating structure. According to the above mentioned simulation results (Yue et al. 2010; Liu et al. 2010) the Abel retrieval method underestimates the electron density underneath the EIA crests; hence, it may degrade the electron density responses but cannot generate the vertically propagating response. Additionally, the LT dependence of the error in the retrieved electron density indicates that mainly the migrating ionospheric response could be affected. The nonmigrating electron density responses are however the main focus of this paper because they are responsible for the ionospheric WN4/WN3 longitude structures.

Recently Chu et al. (2010) have compared the N_mE electron density retrieved by COSMIC satellites with ground-based ionosonde peak values of E region in different latitudinal ranges and different seasons for 2007–2009. The authors found that no matter what season and latitudes are considered, the mean COSMIC N_mE tends to be constantly greater than the ionosonde measurements. This comparison indicates that there is a systematic error in retrieved E-region electron density. The data analysis method used in the paper however filters very efficiently each systematic error. The reason is that such type of errors will affect mainly the constant term (mean electron density) in the decomposition. This parameter is not considered in this study.

Very recently Perrone et al. (2011) have compared the COSMIC N_mE data with the ionosonde measurements at Rome and Gibilmanna (Sicily) for some months of 2006–2007. Italy is completely located at the artificially density enhancement area due to the use of

the Abel retrieval method (Yue et al. 2010 and Liu et al. 2010). The authors found that particularly for the summer months the COSMIC N_mE data turn out to be close to the blanketing frequency f_bEs. Therefore, the sporadic E layers which permanently exist during the summer at middle latitudes strongly contribute to the COSMIC N_mE measurements. Having in mind the contribution of the tides for producing not only the tidal ion layers (Mathews and Sporadic 1998) but also the wind shear for the normal sporadic E layers (Pancheva et al. 2003; Haldoupis et al. 2004, 2006; Haldoupis and Pancheva 2006; Arras et al. 2009) then the ionospheric tidal response seen in the E-region heights could be related to the sporadic E-layer variability as well.

At this stage we may conclude with confidence that the bottom level ionospheric tidal response is real one but its quantitative description has to be accepted with some caution. It is worth noting that the retrieval error problem is too complex and needs to be seriously investigated in future.

This overview study has demonstrated that the application of one and the same data analysis method to the global atmospheric (SABER/TIMED temperatures) and ionospheric (COSMIC electron density) satellite measurements provides an opportunity for a detailed study of the atmosphere-ionosphere coupling by atmospheric waves. The main features of the latitude and altitude structures of the ionospheric nonmigrating tidal response can be summarized as follows:

- The latitude structure of the ionospheric response for heights up to 450–500 km is distributed at both sides of the dip equator at about $\pm 30°$ modip latitude; above 500 km the response is approximately confined to the equator.
- Two altitude regions of enhanced electron density response are found: an upper level response (above 300 km), which usually maximizes near 400–450 km, and a bottom level one (at below 250 km); the two regions are separated by a narrow altitude zone with no tidal response.
- The bottom level response is composed of two parts: a tropical response, near $\pm 30°$ modip latitude, e.g. just underneath the EIA, and a response over the dip equator (the second is not well evident in all nonmigrating tidal responses). While the tropical response maximizes near 200–230 km height that over the equator amplifies at lower levels, near 120–150 km.
- The phase structures at both altitude regions are very different in the tropics: while in the upper level response there is no vertical phase structure, at the bottom level one there is such a structure; over the dip equator however the phase structure at both altitude regions is the same.
- The different phase structures of the ionospheric response in both altitude regions suggests: (i) the upper level response is mainly due to the DE3/DE2 modulated vertical plasma drift, and (ii) the lower level response is complex and probably is caused by more than one mechanism.

The present paper provided also new experimental results which give an explanation why the WN4 and partly WN3 longitude structures are so prominent pattern in the ionosphere. We presented evidence indicating that:

- WN4 longitude structure is most probably caused at least by the combined action of DE3, SE2 and SPW4. The combined electron density variability is almost two times stronger than that generated only by DE3.
- WN3 longitude structure is caused at least by the combined action of DE2, DW4, SE1 and SPW3. The combined electron density variability is almost 1.5 times stronger than that generated only by DE2.

The paper presented also the global distribution and temporal variability of the sun-synchronous 24-h (DW1), 12- (SW2) and 8-h (TW3) electron density oscillations. They are produced by a combination of the diurnal variability (an its harmonics as well) of the photo ionization which depends on the solar zenith angle and the effect of the migrating diurnal, semidiurnal and terdiurnal tides forced from below. The main results can be summarized as follows:

- While the latitude and altitude structure of the ionospheric SW2 response is predominantly shaped by the migrating SW2 tide forced from below the DW1 response is mainly due to daily variability of the photo-ionization.
- The peculiar vertical structure of the ionospheric TW3 response, indicating downward/upward phase progression, hints at possible coupling between the SW2 tide forced from below and the diurnal variability of the electron density, i.e. at ion-neutral momentum coupling.

Despite some progress in investigating the ionospheric response to the atmospheric tides forced from below there are still observational results which need further explanations. For example, it is not clear why the bottom level response over the equator is not vertically propagating one, or why the electron density TW3 response does not correspond to the neutral wind and temperature TW3 upward energy propagation in the lower-middle thermosphere (up to $\sim$300 km altitude), etc. The answer of these and other questions cannot be found only from the analysis and combination of satellite and ground based measurements; it needs further detailed numerical simulations as well.

In conclusion, we note that by means of a detailed analysis of the SABER temperature tides and their global COSMIC electron density responses, we presented valuable and strong experimental evidence that confirms the new paradigm in upper atmospheric and ionospheric physics—that the entire ionosphere regularly responds to the troposphere and stratosphere. These results highlight the importance of understanding the variability of the lower atmospheric weather systems and the possible predictability of the ionospheric response to them. Additionally, the ionospheric tidal diagnostics presented in this overview paper provides the necessary observational constraints for the numerical simulations.

References

M. Angelats i Coll, J.M. Forbes, Nonlinear interactions in the upper atmosphere: the $s = 1$ and $s = 3$ nonmigrating semidiurnal tides. J. Geophys. Res. (2002). doi:10.1029/2001JA900179

C. Arras, Ch. Jacobi, J. Wicker, Semidiurnal tidal signature in sporadic E occurrence rates derived from GPS radio occultation measurements at midlatitudes. Ann. Geophys. **27**, 2555–2563 (2009)

F. Azpilicueta, C. Brunini, S.M. Radicella, Global ionospheric maps from GPS observations using modip latitude. Adv. Space Res. **38**, 2324–2331 (2006)

L. Bankov, R. Heelis, M. Parrot, J.-J. Berthelier, P. Marinov, A. Vassileva, WN4 effect on longitudinal distribution of different ion species in the topside ionosphere at low latitudes by means of DEMETER, DMSP-F13 and DMSP-F15 data. Ann. Geophys. **27**, 1–10 (2009)

N.P. Benkova, M.G. Deminov, A.T. Karpachev, N.A. Kochenova, Yu.V. Kusnerevsky, V.V. Migulin, S.A. Pulinets, M.D. Fligel, Longitude features shown by topside sounder data and their importance in ionospheric mapping. Adv. Space Res. **10**, 857–866 (1990)

P.S. Brahmanandam, Y.-H. Chu, K.-H. Wu, H.-P. Hsia, C.-L. Su, G. Uma, Vertical and longitudinal electron density structures of equatorial E- and F-regions. Ann. Geophys. **29**, 81–89 (2011)

S. Chapman, R.S. Lindzen, *Atmospheric Tides: Thermal and Gravitational* (Gordon and Breach, New York, 1970), p. 200

C.-Z. Cheng, Y.-H. Kuo, R.A. Anthes, L. Wu, Satellite constellation monitors global and space weather. Eos Trans. AGU **87**, 166–167 (2006)

Y.-H. Chu, K.-H. Wu, C.-L. Su, Reply to comment by Lei et al. on "A new aspect of ionospheric E region electron density morphology". J. Geophys. Res. **115**, A07314 (2010). doi:10.1029/2010JA015334

S.L. England, T.J. Immel, E. Sagawa, S.B. Henderson, M.E. Hagan, S.B. Mende, H.U. Frey, C.M. Swenson, L.J. Paxton, The effect of atmospheric tides on the morphology of the quiet-time post-sunset equatorial ionospheric anomaly. J. Geophys. Res. **111**, A10S19 (2006a). doi:10.1029/2006JA011795

S.L. England, S. Maus, T.J. Immel, S.B. Mende, Longitudinal variation of the E-region electric fields caused by atmospheric tides. Geophys. Res. Lett. **33**, L21105 (2006b). doi:10.1029/2006GL027465

S.L. England, X. Zhang, T.J. Immel, J.M. Forbes, R. DeMajistre, The effect of non-migrating tides on the morphology of the equatorial ionospheric anomaly: seasonal variability. Earth Planets Space **61**, 493–503 (2009)

S.L. England, T.J. Immel, J.D. Huba, M.E. Hagan, A. Maute, R. DeMajistre, Modeling of multiple effects of atmospheric tides on the ionosphere: an examination of possible coupling mechanisms responsible for the longitudinal structure of the equatorial ionosphere. J. Geophys. Res. **115**, A05308 (2010). doi:10.1029/2009JA014894

B.G. Fejer, J.W. Jensen, S.-Y. Su, Quiet time equatorial F region vertical plasma drift model derived from ROCSAT-1 observations. J. Geophys. Res. **113**, A05304 (2008). doi:10.1029/2007JA012801

J.M. Forbes, R.G. Roble, C. Fesen, Accelerating, heating and compositional mixing of the thermosphere due to upward propagating tides. J. Geophys. Res. **98**(A1), 311–321 (1993). doi:10.1029/1992JA00442

J.M. Forbes, J. Russell, S. Miyahara, X. Zhang, S. Palo, M. Mlynczak, C.J. Mertens, M.E. Hagan, Troposphere-thermosphere tidal coupling as measure by the SABER instrument on TIMED during July-September 2002. J. Geophys. Res. **111**, A10S06 (2006). doi:10.1029/2005JA011492

J.M. Forbes, X. Zhang, S. Palo, J. Russell, C.J. Mertens, M. Mlynczak, Tidal variability in the ionospheric dynamo region. J. Geophys. Res. **113**, A02310 (2008). doi:10.1029/2007JA012737

T.J. Fuller-Rowell, R.A. Akmaev, F. Wu et al., Impact of terrestrial weather on the upper atmosphere. Geophys. Res. Lett. **35**, L09808 (2008). doi:10.1029/2007GL032911

M.E. Hagan, Comparative effects of migrating solar sources on tidal signatures in the middle and upper atmosphere. J. Geophys. Res. **101**(D16), 21213–21222 (1996)

M.E. Hagan, J.M. Forbes, Migrating and nonmigrating diurnal tides in the middle and upper atmosphere excited by tropospheric latent heat release. J. Geophys. Res. **107**, 4754 (2002). doi:10.1029/2001JD001236

M.E. Hagan, J.M. Forbes, Migrating and nonmigrating semidiurnal tides in the upper atmosphere excited by tropospheric latent heat release. J. Geophys. Res. **108**(A2), 1062 (2003). doi:10.1029/2002JA009466

M.E. Hagan, A. Maute, R.G. Roble, A.D. Richmond, T.J. Immel, S.L. England, Connections between deep tropical clouds and the Earth's ionosphere. Geophys. Res. Lett. **34**, L20109 (2007). doi:10.1029/2007GL030142

M.E. Hagan, A. Maute, R.G. Roble, Tropospheric tidal effects on the middle and upper atmosphere. J. Geophys. Res. **114**, A01302 (2009). doi:10.1029/2008JA013637

C. Haldoupis, D. Pancheva, N.J. Mitchell, A study of tidal and planetary wave periodicities present in mid-latitude sporadic E layers. J. Geophys. Res. **109**, A02302 (2004). doi:10.1029/2003JA010253

C. Haldoupis, C. Meek, N. Christakis, D. Pancheva, A. Bourdillon, Ionogram height-time-intensity observations of descending sporadic E layers. J. Atmos. Sol.-Terr. Phys. **68**, 539–557 (2006)

C. Haldoupis, D. Pancheva, Terdiurnal tide-like variability in sporadic E layers. J. Geophys. Res. **111**, A07303 (2006). doi:10.1029/2005JA011522

K. Hamilton, Latent heat release as a possible forcing mechanism for atmospheric tides. Mon. Weather Rev. **109**, 3–17 (1981)

W.A. Hartman, R.A. Heelis, Longitudinal variations in the equatorial vertical drift in the topside ionosphere. J. Geophys. Res. **112**, A03305 (2007). doi:10.1029/2006JA011773

K. Häusler, H. Lühr, Nonmigrating tidal signals in the upper thermospheric zonal wind at equatorial latitudes as observed by CHAMP. Ann. Geophys. **27**, 2643–2652 (2009)

R.A. Heelis, Electrodynamics in the low and middle latitude ionosphere: a tutorial. J. Atmos. Sol.-Terr. Phys. **66**, 825–838 (2004)

F.T. Huang, H.G. Mayr, C.A. Reber, T. Killeen, J.M. Russell, M. Mlynczak, W. Skinner, J.G. Mengel, Diurnal variations of temperature and winds inferred from TIMED and UARS measurements. J. Geophys. Res. **111**, A10S04 (2006a). doi:10.1029/2005JA011426

F.T. Huang, H.G. Mayr, C.A. Reber, J.M. Russell, M. Mlynczak, J.G. Mengel, Stratospheric and mesospheric temperature variations for quasi-biennial and semiannual (QBO and SAO) oscillations based on measurements from SABER (TIMED) and MLS (UARS). Ann. Geophys. **24**, 2131–2149 (2006b)

T.J. Immel, E. Sagawa, S.L. England, S.B. Henderson, M.E. Hagan, S.B. Mende, H.U. Frey, C.M. Swenson, L.J. Paxton, Control of equatorial ionospheric morphology by atmospheric tides. Geophys. Res. Lett. **33**, L15108 (2006). doi:10.1029/2006GL026161

M.C. Jeruchim, P. Balaban, K.S. Shanmugan, *Simulation of Communication Systems: Modeling, Methodology and Techniques* (Kluwer Academic Plenum Publishers, Dordrecht, 2000), pp. 397–399

H. Jin, Y. Miyoshi, H. Fujiwara, H. Shinagawa, Electrodynamics of the formation of ionospheric wave number 4 longitudinal structure. J. Geophys. Res. **113**, A09307 (2008). doi:10.1029/2008JA013301

H. Jin, Y. Miyoshi, H. Fujiwara, H. Shinagawa, K. Terada, N. Terada, M. Ishii, Y. Otsuka, A. Saito, Vertical connection from the tropospheric activities to the ionospheric longitudinal structure simulated by a new Earth's whole atmosphere-ionosphere coupled model. J. Geophys. Res. **116**, A01316 (2011). doi:10.1029/2010JA015925

A.T. Karpachev, Characteristics of the global longitudinal effect in the night-time equatorial anomaly. Geomagn. Aeron. **28**(1), 46–49 (1988)

M.C. Kelley, V.K. Wong, N. Aponte, C. Coker, A.J. Mannucci, A. Komjathy, Comparison of COSMIC occultation-based electron density profiles and TIP observations with Arecibo incoherent scatter radar data. Radio Sci. **44**, RS4011 (2009). doi:10.1029/2008RS004087

H. Kil, R. DeMajistre, L.J. Paxton, Y. Zhang, Nighttime F-region morphology in the low and middle latitudes seen from DMSP F15 and TIMED/GUVI. J. Atmos. Sol.-Terr. Phys. **68**, 1672–1681 (2006)

H. Kil, S.-J. Oh, M. Kelley, L. Paxton, S. England, E. Talaat, K.-W. Min, S.-Y. Su, Longitudinal structure of the vertical $E \times B$ drift and ion density seen from ROCSAT-1. Geophys. Res. Lett. **34**, L14110 (2007). doi:10.1029/2007GL030018

H. Kil, E.R. Talaat, S.-J. Oh, L.J. Paxton, S.L. England, S.-Y. Su, The wave structures of the plasma density and vertical E × B drift in low-latitude F region. J. Geophys. Res. **113**, A09312 (2008). doi:10.1029/2008JA013106

N.A. Kochenova, Longitudinal variations of the equatorial ionosphere according to Intercosmos-19 data. Geomagn. Aeron. **21**(1), 142–144 (1987)

N.A. Kochenova, Longitudinal variations of $N(h)$ profiles at the magnetic equator. Geomagn. Aeron. **28**(1), 144–146 (1988)

A.K.H. Kong, P.A. Charles, E. Kuulkers, Long-term X-ray variability in GX 354-0. New Astron. **3**(5), 301–307 (1998)

Y.-H. Kuo, T.-K. Wee, S. Sokolovskiy, C. Rocken, W. Schreiner, D. Hunt, R.A. Anthes, Inversion and error estimation of GPS radio occultation data. J. Meteorol. Soc. Jpn. **82**(1B), 507–531 (2004)

J. Lei, S. Syndergaard, A.G. Burns et al., Comparison of COSMIC ionospheric measurements with ground-based observations and model predictions: Preliminary results. J. Geophys. Res. **112**, A07308 (2007). doi:10.1029/2006JA012240

J. Lei, J.P. Thayer, J.M. Forbes, Q. Wu, C. She, W. Wan, W. Wang, Ionosphere response to solar wind high-speed streams. Geophys. Res. Lett. **35**, L19105 (2008). doi:10.1029/2008GL035208

C.H. Lin, W. Wang, M.E. Hagan, C.C. Hsiao, T.J. Immel, M.L. Hsu, J.Y. Liu, L.J. Paxton, T.W. Fang, C.H. Liu, Plausible effect of atmospheric tides on the equatorial ionosphere observed by the FORMOSAT-3/COSMIC: three-dimensional electron density structures. Geophys. Res. Lett. **34**, L11112 (2007a). doi:10.1029/2007GL029265

C.H. Lin, C.C. Hsiao, J.Y. Liu, C.H. Liu, Longitudinal structure of the equatorial ionosphere: time evolution of the four-peaked EIA structure. J. Geophys. Res. **112**, A12305 (2007b). doi:10.1029/2007JA012455

H. Liu, M. Yamamoto, H. Lühr, Wave-4 pattern of the equatorial mass density anomaly: a thermospheric signature of tropical deep convection. Geophys. Res. Lett. **36**, L18104 (2009). doi:10.1029/2009GL039865

J.Y. Liu, C.Y. Lin, C.H. Lin, H.F. Tsai, S.C. Solomon, Y.Y. Sun, T. Lee, W.S. Schreiner, Y.H. Kuo, Artificial plasma caves in the low-latitude ionosphere results from the radio occultation inversion of the FORMOSAT-3/COSMIC. J. Geophys. Res. (2010). doi:10.1029/2009JA015079

H. Lühr, K. Häusler, C. Stolle, Longitudinal variation of F region electron density and thermospheric zonal wind caused by atmospheric tides. Geophys. Res. Lett. **34**, L16102 (2007). doi:10.1029/2007GL030639

H. Lühr, M. Rother, K. Häusler, P. Alken, S. Maus, Influence of nonmigrating tides on the longitudinal variations of the equatorial electrojet. J. Geophys. Res. **113**, A08313 (2008). doi:10.1029/2008JA013064

J.D. Mathews, E. Sporadic, Current views and recent progress. J. Atmos. Sol.-Terr. Phys. **60**, 413–435 (1998)

C. McLandress, W.E. Ward, Tidal/gravity wave interactions and their influence on the large scale dynamics of the middle atmosphere: model results. J. Geophys. Res. **99**, 8139–8156 (1994)

C.J. Mertens et al., Retrieval of mesospheric and lower thermospheric kinetic temperature from measurements of CO_2 15 μm earth limb emission under non-LTE conditions. Geophys. Res. Lett. **28**, 1391–1394 (2001)

C.J. Mertens et al., SABER observations of mesospheric temperature and comparisons with falling sphere measurements taken during the 2002 summer MaCWINE campaign. Geophys. Res. Lett. **31**, J03105 (2004). doi:10.1029/2003GL018605

P. Mukhtarov, D. Pancheva, B. Andonov, Global structure, seasonal and interannual variability of the migrating diurnal tide seen in the SABER/TIMED temperatures between 20 and 120 km. J. Geophys. Res. **114**, A02309 (2009). doi:10.1029/2008JA013759

P. Mukhtarov, D. Pancheva, Global ionospheric response to nonmigrating DE3 and DE2 tides forced from below. J. Geophys. Res. (2011). doi:10.1029/2010JA016099

J. Oberheide, M.E. Hagan, R.G. Roble, D. Offermann, Sources of nonmigrating tides in the tropical middle atmosphere. J. Geophys. Res. **107**, 4567 (2002). doi:10.1029/2002JD002220

J. Oberheide, Q. Wu, T.L. Killeen, M.E. Hagan, R.G. Roble, Diurnal nonmigrating tides from TIMED Doppler Interferometer wind data: monthly climatologies and seasonal variations. J. Geophys. Res. **111**, A10S03 (2006). doi:10.1029/2005JA011491

J. Oberheide, Q. Wu, T.L. Killeen, M.E. Hagan, R.G. Roble, A climatology of nonmigrating semidiurnal tides from TIMED Doppler Interferometer (TIDI) wind data. J. Atmos. Sol.-Terr. Phys. **69**, 2203–2218 (2007)

J. Oberheide, J.M. Forbes, Tidal propagation of deep tropical cloud signatures into the thermosphere from TIMED observations. Geophys. Res. Lett. **35**, L04816 (2008). doi:10.1029/2007GL032397

J. Oberheide, J.M. Forbes, K. Haüsler, Q. Wu, S.L. Bruinsma, Tropospheric tides from 80–400 km: propagation, inter-annual variability and solar cycle effects. J. Geophys. Res. **114**, D00I05 (2009). doi:10.1029/2009JD012388

J. Oberheide, J.M. Forbes, X. Zhang, S.L. Bruinsma, Wave-driven variability in the ionosphere-thermosphere-mesosphere system from TIMED observations: what contributes to the "wave4"? J. Geophys. Res. **116**, A01306 (2011). doi:10.1029/2009JA015911

D. Pancheva, C. Haldoupis, C. Meek, A. Manson, N. Mitchell, Evidence for a role of modulated atmospheric tides in the dependence of sporadic E layers on planetary waves. J. Geophys. Res. **108**(A5), 1176 (2003). doi:10.1029/2002JA009788

D. Pancheva, P. Mukhtarov, B. Andonov, Nonmigrating tidal activity related to the sudden stratospheric warming in the Arctic winter of 2003/2004. Ann. Geophys. **27**, 975–987 (2009a)

D. Pancheva, P. Mukhtarov, B. Andonov, Global structure, seasonal and interannual variability of the migrating semidiurnal tide seen in the SABER/TIMED temperatures (2002–2007). Ann. Geophys. **27**, 687–703 (2009b)

D. Pancheva, P. Mukhtarov, B. Andonov, N.J. Mitchell, J.M. Forbes, Planetary waves observed by TIMED/SABER in coupling the stratosphere-mesosphere-lower thermosphere during the winter of 2003/2004: Part 1, Comparison with the UKMO temperature results. J. Atmos. Sol.-Terr. Phys. **71**, 61–74 (2009c)

D. Pancheva, P. Mukhtarov, B. Andonov, Reply to Manson et al.'s comment on "Global structure, seasonal and interannual variability of the migrating semidiurnal tide seen in the SABER/TIMED temperatures (2002–2007)". Ann. Geophys. **28**, 677–685 (2010a)

D. Pancheva, P. Mukhtarov, B. Andonov, Global distribution, seasonal and interannual variability of the eastward propagating tides seen in the SABER/TIMED temperatures (2002–2007). Adv. Space Res. **46**, 257–274 (2010b). doi:10.1016/j.asr.2010.03.026

D. Pancheva, P. Mukhtarov, Strong evidence for the tidal control on the longitudinal structure of the ionospheric F-region. Geophys. Res. Lett. **37**, L14105 (2010). doi:10.1029/2010GL044039

D. Pancheva, P. Mukhtarov, Atmospheric tides and planetary waves: recent progress based on SABER/TIMED, in *IAGA Special Sopron Book Series 2, Aeronomy of the Earth's Atmosphere and Ionosphere*, ed. by M. Abdu, D. Pancheva (Springer, Berlin, 2011), pp. 19–56, doi:10.1007/978-94-007-0326-1

N.M. Pedatella, J.M. Forbes, J. Oberheide, Intra-annual variability of the low-latitude ionosphere due to nonmigrating tides. Geophys. Res. Lett. **35**, L18104 (2008). doi:10.1029/2008GL035332

L. Perrone, A.V. Mikhailov, L.P. Korsunova, FORMOSAT-3/COSMIC E region observations and daytime f_oE at middle latitudes. J. Geophys. Res. **116**, A06307 (2011). doi:10.1029/2010JA016411

S.M. Radicella, R. Leitinger, The evolution of the DGR approach to model electron density profiles. Adv. Space Res. **27**(1), 35–40 (2001)

K. Rawer, in *Meteorological and Astronomical Influences on Radio Wave Propagation*, ed. by B. Landmark (Oxford, Pergamon Press, 1963), pp. 221–250

K. Rawer (ed.), *Encyclopedia of Physics, Geophysics III, Part VII* (Springer, Berlin, 1984), pp. 389–391

E.E. Remsberg, B.T. Marshall, M. García-Comas, D. Krueger, G.S. Lingenfelser, J. Martin-Torres, M.G. Mlynczak, J.M. Russell, A.K. Smith, Y. Zhao, C. Brown, L.L. Gordley, M.J. Lopez-Gonzales, M. Lopez-Puertas, C.-Y. She, M.J. Taylor, R.E. Thompson, Assessment of the quality of the Version 1.07 temperature-versus-pressure profiles of the middle atmosphere from TIMED/SABER. J. Geophys. Res. **113**, D17101 (2008). doi:10.1029/2008JD0100113

Z. Ren, W. Wan, L. Liu, B. Zhao, Y. Wei, X. Yue, R.A. Heelis, Longitudinal variations of electron temperature and total ion density in the sunset equatorial topside ionosphere. Geophys. Res. Lett. **35**, L05108 (2008). doi:10.1029/2007GL032998

Z. Ren, W. Wan, L. Liu, J. Xiong, Intra-annual variation of wavenumber-4 structure of vertical $E \times B$ drifts in the equatorial ionosphere seen from ROCSAT-1. J. Geophys. Res. (2009). doi:10.1029/2009JA014060

Z. Ren, W. Wan, J. Xiong, L. Liu, Simulated wavenumber 4 structure in the equatorial F region vertical plasma drifts. J. Geophys. Res. **115**, A05301 (2010). doi:10.1029/2009JA014746

Z. Ren, W. Wan, L. Liu, Y. Cheng, H. Le, Equinoctial asymmetry of ionospheric vertical plasma drifts and its effect on F-region plasma density. J. Geophys. Res. **116**, A02308 (2011). doi:10.1029/2010JA016081

A.D. Richmond, The ionospheric wind dynamo: effects of its coupling with different atmospheric regions, in *The Upper Mesosphere and Lower Thermosphere: A Review of Experiments and Theory*, ed. by R.M. Johnson, T.L. Killeen. Geophys. Monogr. Ser., vol. 87 (AGU, Washington, 1995), pp. 49–65

H. Rishbeth, I.C.F. Müller-Wodarg, L. Zou, T.J. Fuller-Rowell, G.H. Millward, R.J. Moffett, D.W. Idenden, A.D. Aylward, Annual and semiannual variations in the ionospheric F2-layer: II. Physical discussion. Ann. Geophys. **18**, 945–956 (2000)

R.G. Roble, The NCAR thermosphere-ionosphere-mesosphere-electrodynamics general circulation model, in *STEP Handbook on Ionospheric Models*, ed. by R.W. Schunk (Utah State Univ., Logan, 1996), pp. 207–216

R.G. Roble, On the feasibility of developing a global atmospheric model extending from the ground to the exosphere, in *Atmospheric Science Across the Stratopause*, ed. by D.E. Siskind, S.D. Eckermann, M.E. Summers. Geophys. Monogr. Ser., vol. 123 (AGU, Washington, 2000), pp. 53–67

E. Sagawa, T.J. Immel, H.U. Frey, S.B. Mende, Longitudinal structure of the equatorial anomaly in the nighttime ionosphere observed by IMAGE/FUV. J. Geophys. Res. **110**, A11302 (2005). doi:10.1029/2004JA010848

W.S. Schreiner, S.V. Sokolovskiy, C. Rocken, D.C. Hunt, Analysis and validation of GPS/MET radio occultation data in the ionosphere. Radio Sci. **34**(4), 949–966 (1999)

S.M. Stankov, N. Jakowski, S. Heise, P. Muhtarov, I. Kutiev, R. Warnant, A new method for reconstruction of the vertical electron density distribution in the upper ionosphere and plasmasphere. J. Geophys. Res. **108**(A5), 1164 (2003). doi:10.1029/2002JA009570

G. Thuillier, J.R.H. Wiens, G.G. Shepherd, R.G. Roble, Photochemistry and dynamics in 566 thermospheric intertropical arcs measure by the WIND imaging interferometer on board UARS: 567 A comparison with TIE-GCM simulations. J. Atmos. Sol.-Terr. Phys. **64**, 405–415 (2002)

W. Wan, L. Liu, X. Pi, M.-L. Zhang, B. Ning, J. Xiong, F. Ding, Wavenumber-4 patterns of the total electron content over the low latitude ionosphere. Geophys. Res. Lett. **35**, L12104 (2008). doi:10.1029/2008GL033755

K.H. West, R.A. Heelis, Longitude variations in ion composition in the morning and evening 574 topside equatorial ionosphere near solar minimum. J. Geophys. Res. **101**, 7951–7960 (1996)

C.R. Williams, S.K. Avery, Diurnal nonmigrating tidal oscillations forced by deep convective clouds. J. Geophys. Res. **101**, 4079–4091 (1996)

J. Xu, A.K. Smith, H.-L. Liu, W. Yuan, Q. Wu, G. Jiang, M.G. Mlynczak, J.M. Russell III, S.J. Franke, Seasonal and quasi-biennial variations in the migrating diurnal tide observed by Thermosphere, Ionosphere, Mesosphere, Energetics and Dynamics (TIMED). J. Geophys. Res. **114**, D13107 (2009). doi:10.1029/2007JD011298

X. Zhang, J.M. Forbes, M.E. Hagan, J.M. Russell III, S.E. Palo, C.J. Mertens, M.G. Mlynczak, Monthly tidal temperatures 20–120 km from TIMED/SABER. J. Geophys. Res. **111**, A10S08 (2006). doi:10.1029/2005JA011504

X. Zhang, J.M. Forbes, M.E. Hagan, Longitudinal variation of tides in the MLT region: 2. Relative effects of solar radiative and latent heating. J. Geophys. Res. **115**, A06317 (2010). doi:10.1029/2009JA014898

X. Yue, W.S. Schreiner, J. Lei, S.V. Sokolovsky, C. Rocken, D.C. Hunt, Y.-H. Kuo, Error analysis of Abel retrieved electron density profiles from radio occultation measurements. Ann. Geophys. **28**, 217–222 (2010)